Development 140, 861-872 (2013) doi:10.1242/dev.087429

Unusual chromatin status and organization of the inactive X chromosome in murine trophoblast giant cells

Catherine Corbel*, Patricia Diabangouaya, Anne-Valerie Gendrel, Jennifer C. Chow‡ and Edith Heard*

SUMMARY

Mammalian X-chromosome inactivation (XCI) enables dosage compensation between XX females and XY males. It is an essential process and its absence in XX individuals results in early lethality due primarily to extra-embryonic defects. This sensitivity to X-linked gene dosage in extra-embryonic tissues is difficult to reconcile with the reported tendency of escape from XCI in these tissues. The precise transcriptional status of the inactive X chromosome in different lineages has mainly been examined using transgenes or in *in vitro* differentiated stem cells and the degree to which endogenous X-linked genes are silenced in embryonic and extra-embryonic lineages during early postimplantation stages is unclear. Here we investigate the precise temporal and lineage-specific X-inactivation status of several genes in postimplantation mouse embryos. We find stable gene silencing in most lineages, with significant levels of escape from XCI mainly in one extra-embryonic cell type: trophoblast giant cells (TGCs). To investigate the basis of this epigenetic instability, we examined the chromatin structure and organization of the inactive X chromosome in TGCs obtained from ectoplacental cone explants. We find that the *Xist* RNA-coated X chromosome has a highly unusual chromatin content in TGCs, presenting both heterochromatic marks such as H3K27me3 and euchromatic marks such as histone H4 acetylation and H3K4 methylation. Strikingly, *Xist* RNA does not form an overt silent nuclear compartment or Cot1 hole in these cells. This unusual combination of silent and active features is likely to reflect, and might underlie, the partial activity of the X chromosome in TGCs.

KEY WORDS: X-chromosome inactivation, Epigenetics, Mouse development, Trophoblast giant cells

INTRODUCTION

During early mouse development there are two waves of X-chromosome inactivation (XCI) in XX individuals. Imprinted inactivation of the paternal X chromosome (Xp) initiates in early cleavage stage embryos (from the 4-cell stage) and is carried through to the trophectoderm of the blastocyst, being maintained during trophoblast differentiation and in the placenta. In the inner cell mass (ICM) of the blastocyst, the inactive Xp is maintained in primitive endoderm cells, which give rise to the visceral endoderm and yolk sac (Okamoto et al., 2004), but is reactivated in cells that will form the epiblast (Okamoto et al., 2004; Mak et al., 2004). Following reactivation, a second wave of XCI occurs at ~E5.5, affecting either the paternal or the maternal X chromosome at random (Rastan, 1982; Takagi et al., 1982).

Both waves of XCI require the action of the non-coding *Xist* RNA, which coats the X chromosome in *cis* and leads to chromosome-wide gene silencing (Penny et al., 1996; Marahrens et al., 1997) (for reviews, see Augui et al., 2011; Wutz, 2011). *Xist* RNA participates in XCI at several levels. During the initiation of XCI it creates a silent nuclear compartment that excludes the transcription machinery (RNA polymerase II), into which genes are recruited as they become inactivated (Chaumeil et al., 2006). *Xist* RNA coating also leads to the depletion of active chromatin marks, such as H3K4 methylation and histone H3 and H4 acetylation (Jeppesen and Turner, 1993; Chaumeil et al., 2002; Chaumeil et al., 2006), and to the recruitment of repressive histone-modifying complexes, including Polycomb group (PcG) proteins for H3K27me3 and H2AK119ub enrichment, as well as other enzymes that lead to H3K9me2 and H4K20me1 modifications (reviewed by Escamilla-Del-Arenal et al., 2011).

DNA methylation of promoter regions on the inactive X chromosome (Xi) is believed to occur at a later stage. Although the mechanisms underlying the changes in nuclear organization and chromatin structure on the Xi are poorly understood, they are thought to participate in establishing silencing and epigenetic memory. However, their continued presence in different embryonic and extra-embryonic lineages during development has not been explored in detail.

In the embryo proper, XCI is believed to be extremely stable due to multiple epigenetic marks that include chromatin modifications and DNA methylation (Csankovszki et al., 2001), as well as nuclear organization. The imprinted inactive Xp in extra-embryonic tissues has been reported to be less stable than in the embryo proper, based on the lower levels of DNA methylation found at promoters of some X-linked genes and on reporter assays with X-linked transgenes (Sado et al., 2000; Hadjantonakis et al., 2001; Kratzer et al., 1983). Studies of paternal X-linked *lacZ* reporter gene activity suggest that XCI is less sensitive to loss of DNA methylation in the visceral endoderm, an extra-embryonic derivative, than in the embryo proper (Tan et al., 1993; Sado et al., 2000). However, studies with an X-linked *GFP* transgene suggest that the paternally transmitted transgene is prone to reactivation in trophoblast giant cells (TGCs) (Hadjantonakis et al., 2001). XCI in extra-embryonic lineages has been reported to be more dependent on PcG proteins than the embryo proper, with a high degree of X-chromosome reactivation in extra-embryonic tissues leading to premature death of female *Eed* mutant embryos (Wang et al., 2001). This study was again based on an X-linked *GFP* transgene.

The extent to which the behavior of X-linked transgenes can be extrapolated to endogenous X-linked genes is not known. Indeed,

Unité de Génétique et Biologie du Développement, Institut Curie, CNRS UMR 3215, INSERM U934, 26 rue d'Ulm, 75248 Paris Cedex 05, France.

*Authors for correspondence (catherine.corbel@curie.fr; edith.heard@curie.fr)
‡Present address: 307 Westlake Avenue North, Suite 300, Seattle, WA 98109, USA

Accepted 7 December 2012

transgenes may be more labile on the Xi than endogenous genes (Csankovszki et al., 2001). However, little is known about the dynamics of endogenous X-linked gene silencing and the epigenetic status of the Xi in different lineages of postimplantation embryos. RNA fluorescent *in situ* hybridization (FISH) studies on X-linked genes in pre- and peri-implantation embryos showed that XCI is complete by E3.5-4.5 in trophectoderm cells (Patrat et al., 2009) and by ~E6.5 in embryonic mouse tissues (Mak et al., 2004), following reactivation in ICM pre-epiblast cells between E3.5 and E4.5 (Williams et al., 2011) (I. Okamoto and E.H., unpublished). A single-cell analysis of this nature (essential to follow the dynamic changes in gene expression within a complex population of cells) has not so far been performed in postimplantation lineages.

Here, we investigate XCI status *in vivo* on cryostat sections of E6.5-8.0 mouse embryos, blastocyst outgrowths and short-term cultures of ectoplacental cones (EPCs), using nascent RNA FISH. This technique provides a direct readout of gene expression and overcomes issues of long mRNA and protein half-lives. RNA FISH was also combined with immunofluorescence to assess several Xi chromosome-wide features at different stages. We show that XCI is particularly unstable in both primary and secondary TGCs, which are large endoreplicating cells with a role in the diffusion of nutrients and oxygen between maternal and fetal blood and the production of different growth hormones (Hu and Cross, 2010). This incomplete status of inactivity is accompanied by an unusual chromosomal organization and chromatin status. The *Xist* RNA-coated portion of the Xi does not form a silent nuclear compartment and is associated with a combination of both active and inactive histone modifications. Partial re-expression of most genes analyzed was found in TGCs, except for the *G6pd* housekeeping gene, pointing to locus-specific differences in epigenetic status on the Xp in TGCs.

MATERIALS AND METHODS

Mouse embryos

Procedures for handling and experimentation followed ethical guidelines established by the Federation of European Laboratory Animal Science Associations. F1 (C57BL/6 × DBA/2) mice were bred in the Animal Care Facility of the Institut Curie (agreement number: C 75-05-18).

The day on which the vaginal plug was detected was defined as day 0 of gestation (E0). Isolation of E7 EPCs was carried out as previously described (Corbel et al., 2007).

Cryostat sections and sample preparation

Conceptuses were embedded in OCT compound (Tissue-Tek), frozen in liquid N_2, then cut using a CM 1950 cryostat (Leica) into 8 μm sections. Embryos on slides and cultured cells on coverslips were fixed and permeabilized as described (Patrat et al., 2009).

Immunofluorescence and RNA FISH analysis

Immunofluorescence and antibodies were as described (Okamoto et al., 2004), except anti-Atrx (H300, sc-15408, Santa Cruz) and anti-H3K9me2 (MCA-MABI0007-100-EX, Cosmo). L1 RNA was detected using a full-length Tf element (TNC7). Mouse Cot1 DNA (Invitrogen), *Xist* and gene-specific BAC probes are as described (Patrat et al., 2009), except the *Mecp2* probe FOSMID G135P601977A8. Placental lactogen 1 (Pl1; Prl3d1 – Mouse Genome Informatics) was detected using BAC RP23-211I16. Probes were labeled with SpectrumGreen-dUTP, SpectrumRed-dUTP (Vysis) or Cy5-dUTP (Dutscher) by nick translation (Vysis). RNA and DNA FISH experiments were performed as described (Patrat et al., 2009; Chaumeil et al., 2008). For DNA FISH, an RNase treatment was performed for 60 minutes at 37°C prior to denaturation (in 50% formamide/2×SSC at 80°C for 30 minutes). X-chromosome paint probe was from Cambio.

Derivation of TGCs in culture

To generate primary and secondary TGCs, individual E3 blastocysts and individual E7 EPCs, respectively, were grown on glass coverslips (12 mm in diameter, no 1, Marienfeld) in 4-well multidishes (Nunc), each containing 0.5 ml medium [DMEM or RPMI 1640, 10-15% fetal calf serum (Invitrogen), 0.1 mM 2-mercaptoethanol (Sigma) and antibiotics] at 37°C in 5% CO_2 for 4-5 days and 3-4 days, respectively. Female embryos could be distinguished from males by *Xist* RNA FISH: the presence of an *Xist* RNA domain in the nucleus is evidence that the embryo is female.

Fluorescence microscopy

A 200M Axiovert fluorescence microscope (Zeiss) equipped with an ApoTome was used to generate 3D optical sections. Sequential *z*-axis images were collected in 0.3 μm steps. Relative intensity values were determined by line traces made across nuclei using ImageJ (NIH).

Bisulfite treatment and analysis by Sequenom

Genomic DNA was prepared from pooled preparations of male and female secondary TGCs derived from E7 EPCs, from individual E7 embryos and from adult liver as somatic control, using standard methods. Bisulfite conversion of DNA was performed using the Epitect Bisulfite Kit (Qiagen). Bisulfite-converted DNA was amplified using primers for the CpG islands linked to *Mecp2*, *Rnf12* (*Rlim* – Mouse Genome Informatics), *Atrx*, *G6pd* (*G6pdx* – Mouse Genome Informatics) and *Huwe1* and for the 5′UTR of the L1-Tf elements located immediately upstream and downstream of the *Huwe1* gene (Chow et al., 2010). Primers details are given in supplementary material Table S3. PCR products were analyzed by MALDI-TOF mass spectrometry after *in vitro* transcription and specific cleavage by Sequenom (Ehrich et al., 2005). For each amplicon, two male and four female TGCs and three male and five female E7 embryos were analyzed, along with one sample for the somatic control.

RESULTS

X-linked gene activity in early postimplantation (E6.5-8.0) mouse embryos

The degree of XCI in different tissues and at various postimplantation stages (E6.5-8.0) was investigated in embryos on cryostat sections. The transcriptional status of different X-linked genes, as well as the *Xist* RNA coating of the Xi, were assayed by RNA FISH. Four X-linked genes, *Rnf12*, *Kif4*, *Huwe1* and *Atrx*, for which preimplantation kinetics of silencing had been previously described (Patrat et al., 2009), were examined. *Rnf12* and *Kif4* are silenced rapidly (4- to 8-cell stage), whereas *Huwe1* is inactivated more slowly, only being fully silenced by E6.5 in extra-embryonic tissues (Patrat et al., 2009). *Atrx* displays full Xi silencing in the blastocyst, but then undergoes lineage-specific escape from XCI in the trophectoderm-derived extra-embryonic ectoderm at E6.5. We controlled for the efficiency of our RNA FISH detection for these genes on the active X chromosome (Xa) in male postimplantation embryo sections, where gene expression from the Xa could be detected in more than 90% of cells (see supplementary material Table S1). The degree of escape from XCI of these genes was then evaluated in female embryo sections based on the detection of two primary transcript signals, one of which is adjacent to the *Xist* RNA-coated chromosome.

We examined E7 sections, as different lineages of the embryo are readily identifiable at this stage owing to the formation of the ectoplacental and amniotic cavities, the chorion (which is often separated from the EPC) and the allantois, a morphological landmark (Downs and Davies, 1993) that is well developed but not yet fused to the chorion. An example of the data obtained for *Xist* and *Kif4* in an E7 female embryo is shown in Fig. 1A-C. A single *Xist* RNA domain was detected in the overwhelming majority of embryonic and extra-embryonic cells (94%, *n*=296). *Kif4* was expressed from the Xa in the majority of cells in all lineages at this

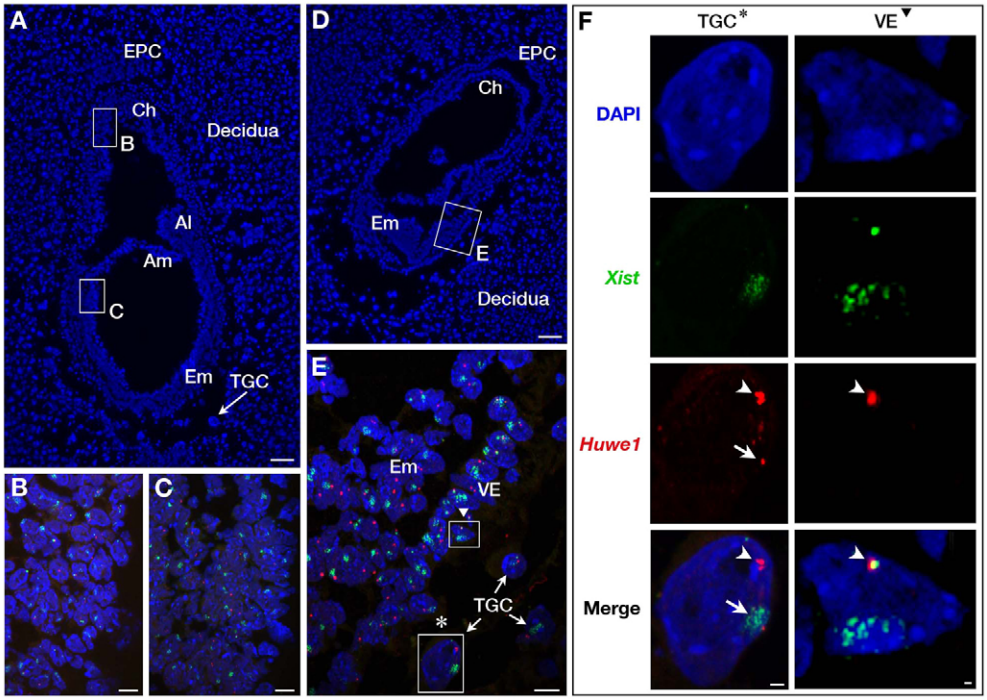

Fig. 1. Expression of *Kif4* and *Huwe1* in E7.0 and E7.5 female embryonic sections. (**A-C**) *Kif4* and *Xist* RNA expression in E7.0 mouse embryos. (A) Longitudinal section of the conceptus passing exactly through the middle axis (DAPI staining); at this stage, the different lineages are easily recognized by their morphology. The embryo and extra-embryonic tissues are surrounded by the decidua (maternal tissue). Boxed regions are shown at higher magnification in B,C. (B,C) RNA FISH for *Xist* (green) and *Kif4* primary transcript (red) showing (B) the two intermingled extra-embryonic lineages of the chorion (Ch) and the EPC and (C) the embryonic lineage. (**D-F**) *Huwe1* and *Xist* RNA expression in E7.5 embryos. (D) Semi-longitudinal section of the conceptus, not passing exactly through the middle axis (DAPI staining), showing the well-differentiated chorion, separated from the EPC. (E) Higher magnification of the boxed regions in D showing *Huwe1* primary transcript (red) and *Xist* RNA (green). (F) Higher magnification of the boxed regions in E showing (left column) a TGC in which *Huwe1* expression is biallelic on both Xi (arrow) and Xa (arrowhead) and (right column) a cell from the VE in which *Huwe1* is monoallelically expressed (Xa, arrowhead) and silent on the *Xist*-coated X chromosome (Xi). Al, allantois; Am, amnios; Ch, chorion; Em, embryo; EPC, ectoplacental cone; VE, visceral endoderm; TGC, trophoblast giant cell. Scale bars: 100 μm in A,D; 10 μm in B,C,E; 2 μm in F.

stage (>95%; Table 1), as was the case for *Rnf12*, *Kif4*, *Huwe1* and *Atrx* examined at E7.0 (Table 1). Very low frequencies of escape from XCI were found in embryonic tissues (<3.5%) at all stages (Table 1). However, higher frequencies of escape from XCI were found particularly in one extra-embryonic tissue: the TGCs. Over 30% of TGCs showed some degree of biallelic *Huwe1* or *Atrx* expression at E7.0 (Table 1). Clusters of punctate signals could be observed by RNA FISH on both the Xa and the *Xist* RNA-coated Xp in these cells (Fig. 2A-C), presumably corresponding to multiple gene copies, as TGCs are polyploid cells that differentiate from diploid trophoblast cells according to a cellular process known as endoreplication (no mitosis and multiple rounds of DNA replication). The degree of endoreplication was variable (see Fig. 1F versus Fig. 2A-C).

We examined X-linked gene expression in TGCs in more detail in E6.5-8 embryo cryosections (Fig. 2). An example of the XCI status of *Huwe1* in different cell types, including TGCs, in an E7.5 embryo is shown in Fig. 1D-F. We did not note any difference in

Table 1. Quantification of *Rnf12*, *Kif4*, *Huwe1* and *Atrx* expression from the Xi in different embryonic and extra-embryonic lineages at E7

	Percentage of cells showing escape[¶]			
Tissue lineage	*Rnf12*	*Kif4*	*Huwe1*	*Atrx*
EPC	0 (*n*=36)	4.8[‡] (*n*=63)	4.65 (*n*=80)	2.0 (*n*=198)
Chorion	0 (*n*=22)	–	6.2 (*n*=61)	22.0 (*n*=122)
TGC	9.4* (*n*=32)	0* (*n*=35)	38.4* (*n*=69)	31.9[§] (*n*=47)
Embryo	2.4 (*n*=42)	3.3 (*n*=36)	2.6 (*n*=42)	0 (*n*=173)
Visceral endoderm	0 (*n*=15)	0 (*n*=65)	7.5 (*n*=108)	0 (*n*=84)

RNA FISH was performed on sections of the E7 conceptus using *Xist* and X-linked probes. The percentage of cells showing expression from the Xi was obtained for *Rnf12* from one embryo (except *TGC, three embryos), *Kif4* and *Huwe1* from two embryos (except *TGC, three embryos) and *Atrx* from three embryos (except [§]TGC, four embryos). *n*, the total number of nuclei analyzed by RNA FISH.
[‡]The embryos analyzed for *Kif4* expression did not enable the EPC to be distinguished from the chorion.
[¶]One *Xist* RNA domain plus biallelic gene expression.

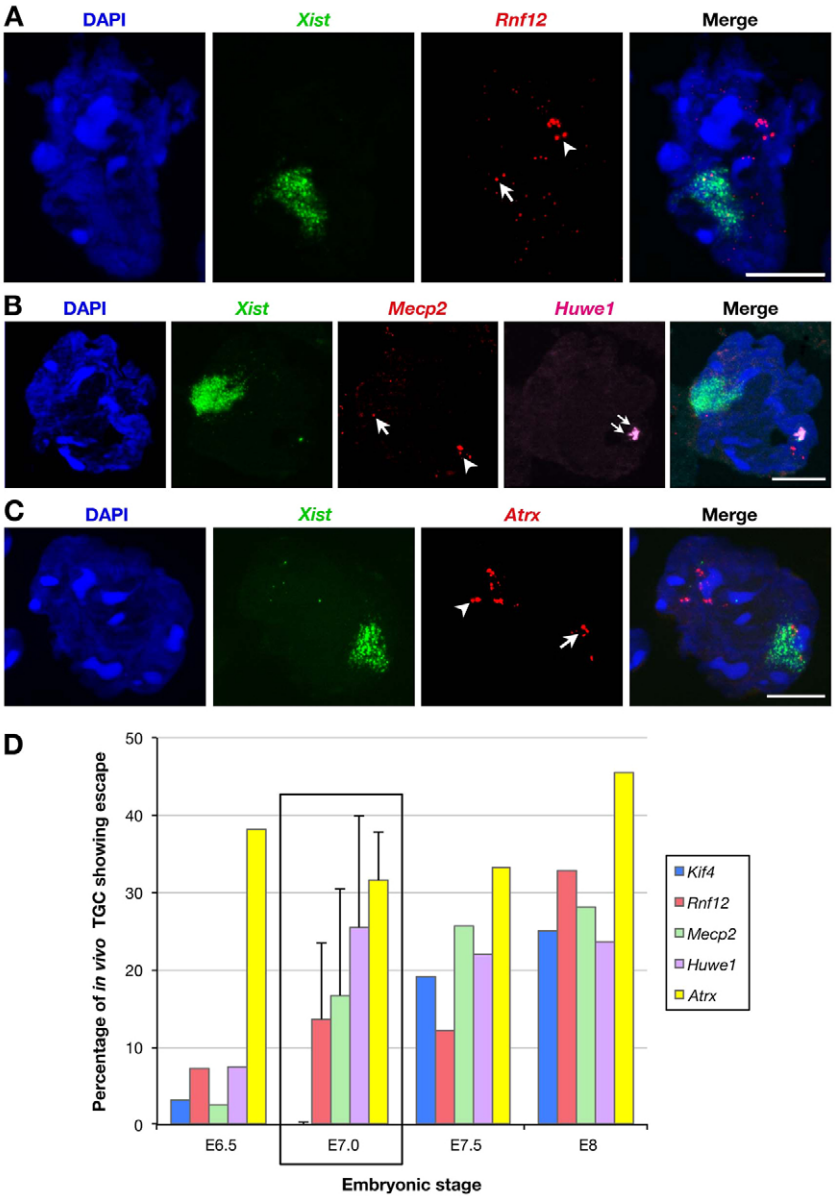

Fig. 2. Biallelic expression of *Kif4*, *Rnf12*, *Mecp2*, *Huwe1* and *Atrx* in TGCs at different postimplantation stages from E6.5 to E8.0. (**A-C**) Examples of *in vivo* TGC nuclei showing XCI escape for three X-linked genes. Shown are *Xist* RNA (green) and each gene exhibiting biallelic expression (red). Arrow, Xi; arrowhead, Xa. (A) *Rnf12* at E7.5. (B) *Mecp2* at E8.0. Note in this particular TGC the biallelic expression of *Mecp2* but not of *Huwe1*. (C) *Atrx* at E7.0. (**D**) Degree of escape from XCI: the percentage of TGCs showing biallelic expression. As at least three embryos were analyzed at E7.0, standard deviations are given for this stage (boxed). At other embryonic stages, the mean for up to three embryos analyzed is given. For full data, see supplementary material Table S2. Scale bars: 10 μm.

the XCI status of TGCs based on their localization in the embryo (either surrounding the EPC or close to the embryo proper). We found that different genes show differences in the timing and extent of escape from XCI in TGCs (Fig. 2D). *Kif4* shows no escape from XCI at E6.5 and E7 but high frequencies at E7.5 (19%) and E8.0 (25%). *Rnf12* displays a low frequency of escape (7-13%) at E6.5-7.5 but much higher frequencies at E8 (30%). By contrast, *Mecp2* exhibits escape as early as E7.0 (>16%). *Huwe1*, which is silenced at E6.5 (Patrat et al., 2009), shows a high frequency of escape from as early as E7 (>25%). *Atrx* escapes at very high frequency from E6.5 (>38%) to E8.0 (>45%) (Fig. 2C; supplementary material Fig. S1E). This is consistent with the lineage-specific escape reported for *Atrx* based on dissociated embryos at E6.5 (Patrat et al., 2009).

Intriguingly, *Atrx* also showed very frequent escape from XCI in the chorion, unlike the other genes examined (Table 1; supplementary material Fig. S1D). Since the Atrx protein has been reported to be highly expressed in the chorion and TGCs of E7 embryos (Garrick et al., 2006) and to be associated with the Xi (Baumann and De La Fuente, 2009), we investigated whether *Atrx* escape from XCI in these tissues might be linked to their increased requirement for Atrx levels. Immunofluorescence using an anti-Atrx antibody (supplementary material Fig. S1A-C) revealed that lineage-specific *Atrx* escape from XCI corresponds to increased protein levels in the chorion and TGCs (supplementary material Fig. S1A). No significant overlap between the *Xist* RNA-coated Xp and Atrx protein staining was observed, however (supplementary material Fig. S1B,C).

In conclusion, our analysis of X-linked gene activity in E6.5-8.0 embryos reveals that XCI is efficiently maintained in embryonic lineages for the *Rnf12*, *Kif4*, *Huwe1* and *Atrx* genes analyzed. However, TGCs clearly show a high rate of escape and, intriguingly, different loci show substantial differences in the timing and degree of escape in these cells. The limited numbers of TGCs in E6.5-8.0 embryos and their large size rendered their analysis challenging in cryosections (supplementary material Table S2; the data per embryo is shown for each gene and each stage). We therefore decided to evaluate the XCI status of X-linked genes and others features of the Xi more systematically using short-term

cultures of primary TGCs derived from the mural trophectoderm of blastocysts and secondary TGCs that are believed to be derived from the polar trophectoderm that gives rise to the EPC.

XCI analysis in primary TGCs cultured from E3 mouse embryos

To examine primary TGCs for their XCI status, blastocysts were removed at E3 and individually cultured. After 4 or 5 days of culture and outgrowth, the ICM was surrounded by large primary TGCs (Carney et al., 1993) (Fig. 3A). X-linked gene activity and *Xist* expression were analyzed by RNA FISH. Only nuclei with a single *Xist* RNA domain were considered (68% of TGCs, *n*=122 from seven female embryos). As in the *in vivo* postimplantation cryosections, several pinpoints of primary transcripts could be detected for the X-linked genes as a result of endoreplication (Fig. 3B).

Very high rates of biallelic expression for *Rnf12* (25.5%), *Atrx* (28.8%), *Mecp12* (42.8%), *G6pd* (36.8%) and *Huwe1* (73%) (Fig. 3B,C) were observed in these primary TGCs. In the case of *Huwe1*, biallelic expression was expected given that in blastocysts it is not yet inactivated, with XCI only occurring at ~E5-6.5 (Patrat et al., 2009). This was also the case for *Mecp2*, which displays only partial XCI (60% biallelic expression) at the E3 blastocyst stage (Patrat et al., 2009). Thus, for these two genes in primary TGCs, incomplete XCI could not be distinguished from escape from XCI following establishment. This contrasts with the situation in postimplantation stages, where we could see that most genes, including *Huwe1* and *Mecp2*, show no/low escape from XCI at E6.5, but show increasing rates of escape in TGCs from E7.0 onward.

Given that the giant cells that we observed to exhibit high levels of escape *in vivo* in E7.0-8.0 sections corresponded not only to primary but also to secondary TGCs at these postimplantation stages, we turned to secondary TGC cultures from early postimplantation embryos.

XCI analysis in secondary TGCs derived from E7 EPCs

To assess the transcriptional and epigenetic status of the Xi in secondary TGCs, short-term cultures of single E7 EPCs were used (supplementary material Fig. S2A-D), as these represent a more physiological situation than trophoblast stem (TS) cell lines and differentiated derivatives, which have been shown to not entirely reflect the epigenetic status of extra-embryonic progenitor cells in the embryo (Rugg-Gunn et al., 2010). To identify TGCs in our EPC cultures, we analyzed placental lactogen 1 (Pl1) expression by RNA FISH. The *Pl1* gene is specifically expressed in both primary and secondary TGCs (Ma and Linzer, 2000) and was found to be expressed in cells derived from EPC cultures after 3 days of culture (supplementary material Fig. S2E). Giant cells (TGCs) could be identified by their characteristically large nuclei that result from endoreplication (Zybina and Zybina, 1996) and were observed mainly at the edges of the culture, adjacent to smaller trophoblast cells (supplementary material Fig. S2B-D).

Using RNA FISH as before, we analyzed gene expression in these short-term cultures. Only cells with two X chromosomes and one *Xist* RNA cloud were considered. Multiple punctate signals were observed by RNA FISH for X-linked genes, consistent with endoreplication in TGCs (Fig. 4A-E), similar to the situation observed in *in vivo* cryosections (Fig. 2; supplementary material Fig. S1E). We therefore focused our subsequent analyses on the larger cells in the population in order to ensure that TGCs were evaluated.

The activity of several X-linked genes including *Rnf12*, *Mecp2*, *Huwe1*, *Atrx* and *G6pd* was assessed in these secondary TGCs

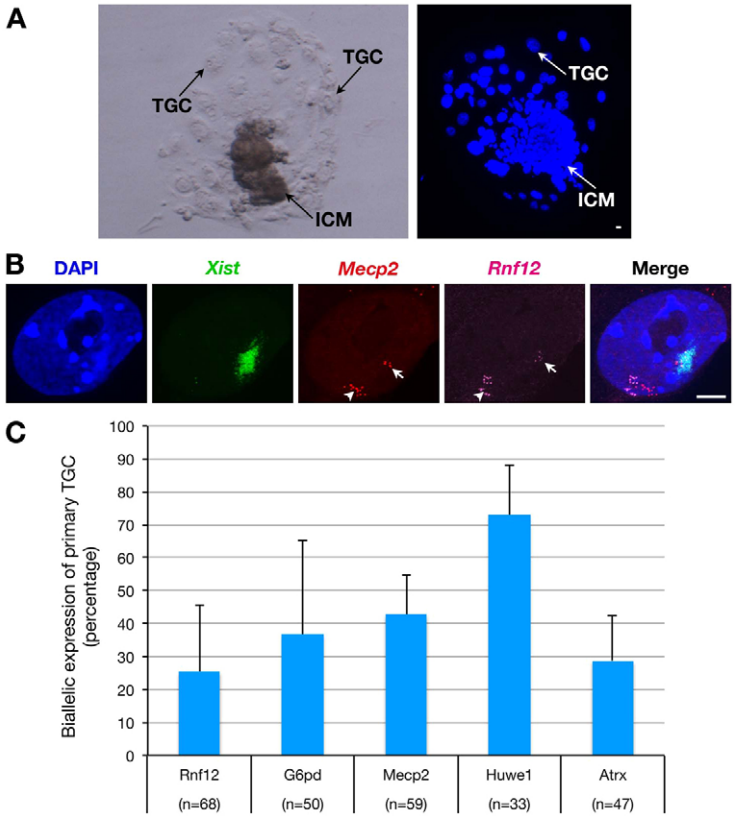

Fig. 3. X-inactivation status of primary female TGCs derived from E3.0 mouse embryos. (**A**) Primary TGC differentiation after 4-5 days of *in vitro* culture of single E3 blastocysts. Phase contrast (left) and DAPI staining (right). Trophoblast giant nuclei are distinct from the small cells of the ICM. (**B**) Example of biallelic expression of *Mecp2* and *Rnf12*: at least one RNA signal close to/within that of *Xist* is detected in addition to that on the Xa. Arrow, Xi; arrowhead, Xa. (**C**) Quantification of biallelic expression of *Rnf12* (six embryos), *G6pd* (five embryos), *Mecp2* (six embryos), *Huwe1* (three embryos) and *Atrx* (two embryos) in primary TGCs. *n*, number of nuclei. Error bars indicate s.d. Scale bars: 10 μm.

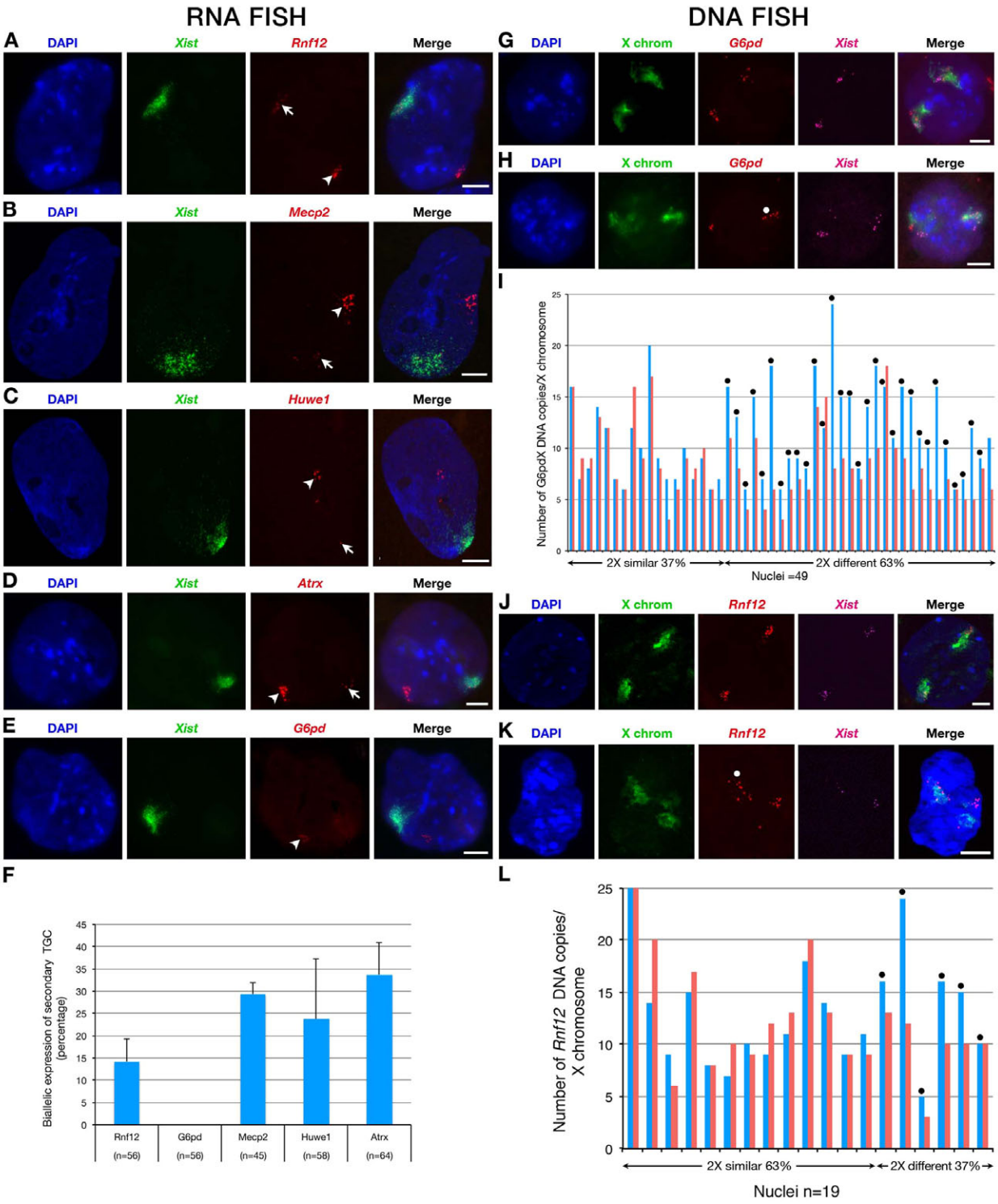

Fig. 4. X-inactivation status of secondary female TGCs derived from E7 EPCs. (**A-E**) Examples of RNA FISH signals in secondary TGCs for each X-linked gene investigated. DAPI (blue), *Xist* RNA (green), gene primary transcript (red). Arrow and arrowhead indicate expression from the Xi and Xa, respectively. Illustrated are biallelic expression of (A) *Rnf12*, (B) *Mecp2*, (C) *Huwe1* and (D) *Atrx* and monoallelic expression of (E) *G6pd*. (**F**) Quantification of biallelic expression. Mean (percentage of nuclei) ± s.d. from two experiments. *n*, number of nuclei. *G6pd* shows no escape from XCI. (**G**,**H**,**J**,**K**) DNA FISH for *G6pd*, *Xist* and *Rnf12* and X-chromosome paint after RNase treatment. (G,H) Examples of cells after *G6pd*/*Xist*/X paint DNA FISH. (G) Similar volumes are occupied by both the Xa and Xi chromosomes. (H) Different volumes occupied by the two X chromosomes. Note that here the *Xist* cluster is well separated from *G6pd*. (**I**) Quantification of *G6pd* DNA copy number for each X chromosome in TGC nuclei (*n*=49) indicating spread clusters on one X (blue) and compacted clusters on the other (red). (J,K) Examples of cells after *Rnf12*/*Xist*/X paint DNA FISH. (J) Similar volumes are occupied by the DNA copies on both X chromosomes. (K) Different volumes are occupied by the DNA copies on each X chromosome. (**L**) Quantification of the number of *Rnf12* DNA copies for each X chromosome in TGC nuclei (*n*=19) indicating spread clusters on one X (blue) and compacted clusters on the other (red). Solid circles (I,L) indicate the X chromosome with spread DNA copies as compared with the other chromosome where they are condensed. Scale bars: 10 μm.

(Fig. 4A-F). *Rnf12*, *Mecp2*, *Huwe1* and *Atrx* showed high rates (15-35%) of escape from XCI. Thus, secondary TGCs derived from E7 EPC short-term cultures display similar rates of escape from XCI as TGCs observed *in vivo* in sections. Intriguingly, *G6pd* displayed no sign of expression whatsoever from the Xi, even though it is robustly detected on the Xa (Fig. 4E).

The number of primary transcript signals associated with the *Xist* RNA-coated X chromosome for genes escaping XCI varied considerably from cell to cell. To assess whether endoreplicated copy number and/or the degree of clustering between copies of expressed genes might differ between the Xa and Xi, we counted the number of RNA signals present on each and evaluated their distribution for each gene. For *Rnf12* and *Atrx*, for example, the majority of nuclei (87.5% and 73%, respectively) have similar numbers of signals on the two X chromosomes (8-20 and 2-15 pinpoints, respectively) but show considerable variability in the distribution of signals, with more dispersed clusters on the Xi than on the Xa in 57% and 37.5% of nuclei, respectively (Fig. 4A). When the number of *Atrx* signals differed between the two X chromosomes, we could not detect any correlation in signal number on the Xa versus the Xi. Dispersal of signals is similar on both X chromosomes (Fig. 4D). Similar variability was found for the other genes analyzed. Fig. 4B illustrates a nucleus in which the number of *Mecp2* signals is lower on the Xi than on the Xa (ten and 20 pinpoints, respectively) with a similar degree of dispersal in both cases. Fig. 4C shows an example in which the number of *Huwe1* signals differs (two on the Xi and ten on the Xa), with dispersal on the Xa in this case.

We evaluated whether endoreplicated genes show differences in copy number or compaction on the Xa versus the Xi and whether such differences might explain the variability between genes in escape from XCI. For example, *Rnf12* escapes XCI in ~15% of TGCs, whereas *G6pd* shows 0% escape – could this be due to a lower endoreplicated copy number in the case of *G6pd*? To address this, DNA FISH for the *Rnf12* and *G6pd* loci was performed (following RNase treatment) and the number and volume occupied by the multiple copies of each locus on the Xa and Xi were assessed. In the case of *G6pd*, differences in compaction were found between the two X chromosomes in two-thirds of nuclei (Fig. 4G-I). For *Rnf12*, one-third of nuclei showed different degrees of compaction on the two X chromosomes (Fig. 4J-L).

We conclude that differences in copy number or degree of compaction on the Xa and Xi are unlikely to explain the different escape rates found between X-linked genes in secondary TGCs.

Chromatin status of the Xi in secondary TGCs

We investigated the possible chromatin basis for the epigenetic instability of X-linked genes on the Xi in secondary TGCs. Levels of DNA methylation at the promoters of the *Mecp2*, *Rnf12*, *Atrx*, *Huwe1* and *G6pd* genes were analyzed in secondary TGCs and somatic tissues using Sequenom (supplementary material Fig. S3). Low levels of DNA methylation were found at all X-linked promoters examined in female TGCs, as compared with control somatic tissues (supplementary material Fig. S3A), consistent with previous reports for *Hprt* and *Msg1* (*Cited1* – Mouse Genome Informatics) in the yolk sac endoderm (Kratzer et al., 1983; Sado et al., 2000). Importantly, the *G6pd* promoter showed similarly low levels of methylation in TGCs to the other gene promoters examined (supplementary material Fig. S3A), even though *G6pd* shows no sign of escape from XCI in TGCs. Thus, although promoters of X-linked genes seem to be less methylated in TGCs relative to somatic cells, as expected, differences in the degree of DNA methylation cannot explain the differences in the propensity for some genes to escape XCI.

We next assessed various histone modifications and associated proteins on the Xi in EPC-derived secondary TGCs. Given the limited TGC numbers, even in EPC short-term cultures we could not use a chromatin immunoprecipitation approach, so instead used combined immunofluorescence and RNA FISH. During both imprinted and random XCI, *Xist* RNA coating the X chromosome is associated with accumulation of Polycomb repressive complex (PRC2) and deposition of the histone mark H3K27me3. In secondary TGCs, 100% of *Xist* RNA domains were enriched for H3K27me3 and the PRC2 protein Eed (Fig. 5A-C). However, another repressive mark, H4K20me1, that has been associated with the Xi during ES cell differentiation, exhibited no significant enrichment on the Xi in secondary TGCs (no enrichment, 74%; partial enrichment, 26%; n=35; data not shown).

We also examined euchromatic histone marks, such as H3K4me2 and H4KAc, both of which are normally depleted on the Xi during XCI (Keohane et al., 1996; Chaumeil et al., 2002; Okamoto et al., 2004; Chaumeil et al., 2006). X-linked chromatin coated by *Xist* RNA exhibited only partial or no hypoacetylation of H4 (Fig. 5D; further examples of partial or no depletion on the Xi are shown in supplementary material Fig. S4A). In the case of H3K4me2 (Fig. 5E,F), partial hypomethylation (54% of nuclei) was observed on the Xi in secondary TGCs and more complete hypomethylation in the remaining nuclei (Fig. 5D; supplementary material Fig. S4B). These patterns of H4Ac and H3K4me2 on the Xi seem to reflect a mixed chromatin status, with a partially inactive signature based on H3K4me2 and a partially active signature based on H4Ac. This situation is very different to that in somatic cells, where close to 100% of cells show an absence of H3K4me2 and H4Ac on the Xi at interphase (Chaumeil et al., 2002). Thus, the Xi in TGCs clearly possesses a rather unusual chromatin status, with a mixture of inactive (H3K27me3 and partial H3K4me2 depletion) and active (H4Ac) marks present simultaneously.

Chromatin status of the Xi in primary TGCs

To assess whether this unusual Xi chromatin organization is found in primary TGCs, we examined the Xi in blastocyst outgrowths using immuno-RNA FISH. Staining for H4Ac and H3K4me2 on the *Xist* RNA-coated chromosome revealed three categories of nuclei showing total, partial or no depletion on the Xi. Similar to secondary TGCs, a large proportion of cells showed acetylation of H4 (18.4% total depletion and 63.2% partial depletion) and H3K4 dimethylation (17.4% total depletion and 52.2% partial depletion) on the *Xist* RNA-coated X chromosome (supplementary material Fig. S5A-C). Heterochromatic marks such as H3K27me3, Eed and H3K9me2 were enriched on the Xi in all primary TGC nuclei (supplementary material Fig. S5D-G), as previously reported for blastocysts (Okamoto et al., 2004; Mak et al., 2004). In conclusion, in primary TGCs the Xi exhibits a similar unusual chromatin status to that found in secondary TGCs, with a mixture of active and inactive marks.

Nuclear organization of the Xi in secondary TGCs

An early feature of XCI is the global depletion of RNA polymerase II (RNA Pol II) and associated transcription factors within the *Xist* RNA domain. This silent compartment is present in almost 100% of cells during the onset of imprinted and random XCI and in the soma (Chaumeil et al., 2006). In embryos, RNA Pol II is excluded from the *Xist* RNA-coated Xp from as early as the 4- to 8-cell stage

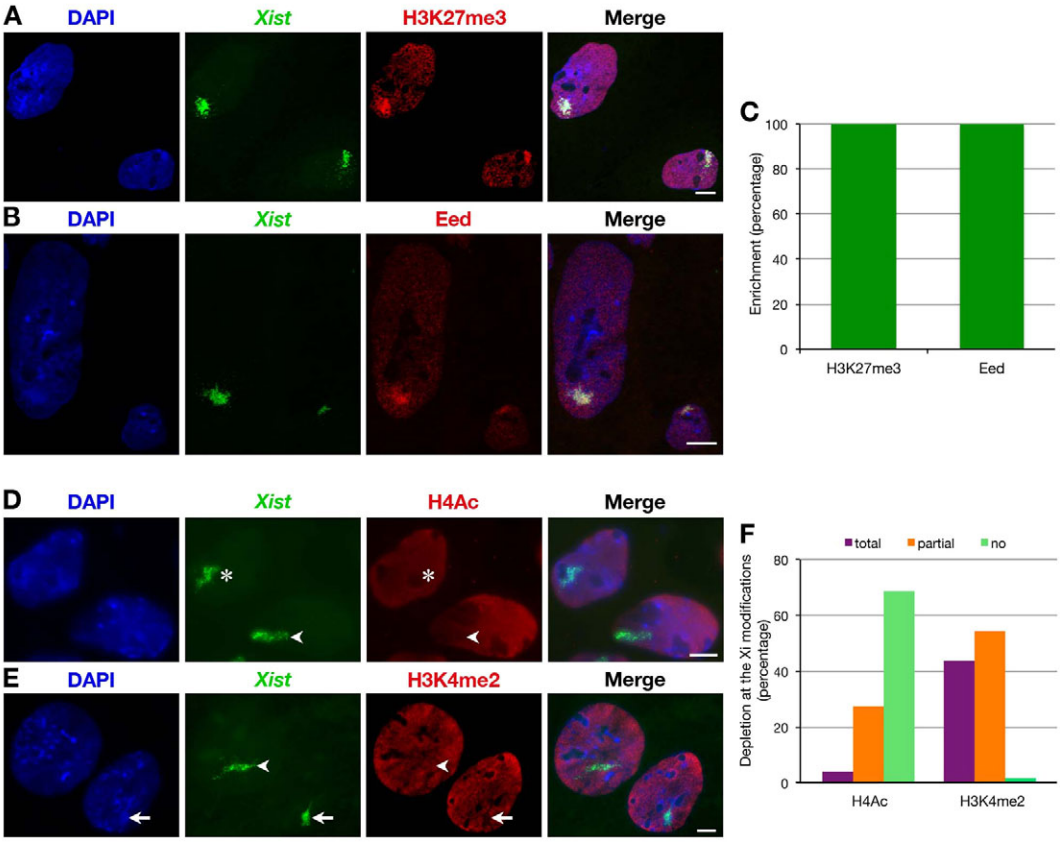

Fig. 5. Chromatin modifications of the Xi in secondary female TGCs derived from E7 EPCs. (A,B,D,E) Representative immunofluorescence images using antibodies (red) combined with *Xist* RNA FISH (green). (**A-C**) Chromatin marks or proteins typically associated with silent chromatin. (A) H3K27me3 (*n*=32) and (B) Eed (*n*=32). (C) Quantification of TGCs with enrichment at the Xi. (**D-F**) Chromatin marks typically associated with active chromatin. (D) Histone hypoacetylation on the Xi illustrating partial depletion (arrowhead) and no H4Ac depletion (asterisk). (E) Partial (arrowhead) and total (arrow) depletion of histone H3K4 dimethylation on the Xi. (F) Quantification of TGCs with total, partial or no depletion at the Xi of H4 acetylation (*n*=139) and H3K4 dimethylation (*n*=57). Scale bars: 10 μm.

(Okamoto et al., 2004). We investigated this feature of XCI in TGCs. In secondary TGCs derived from EPCs (Fig. 6A-D), we found no (35.6% of nuclei) or only partial (62.7%) RNA Pol II exclusion from the *Xist* RNA-coated chromosome (Fig. 6B,C). Similarly, no RNA Pol II exclusion could be detected in 40% of primary TGCs (supplementary material Fig. S6B,C). This enrichment for RNA Pol II on the Xi was similar in pattern to that seen for H3K4me2 and H4Ac and contrasts sharply with the situation in embryonic lineages.

The presence of RNA Pol II on the Xi in TGCs also prompted us to analyze Cot1 RNA depletion, as the Cot1 'hole' is another hallmark of the silent *Xist* RNA compartment (Hall and Lawrence, 2011; Chaumeil et al., 2006). A Cot1 hole was distinctly lacking on the Xi in secondary TGCs (Fig. 6E,F), with Cot1 RNA being clearly detected within the *Xist* RNA domain in almost all TGCs (97.6±2.4%, *n*=108) (Fig. 6G). Furthermore, no Cot1 hole could be detected on the Xi in 40% of the primary TGCs (supplementary material Fig. S6A,C). Similarly, the majority of TGCs showed no or only partial depletion of Cot1 RNA within their *Xist* domain in E7.0 embryos (data not shown).

We also evaluated the expression of specific repeats, in particular of the LINE-1 (L1) family, as our recent work showed that a subset of young LINEs is expressed from the Xi (Chow et al., 2010). Using L1/*Xist* RNA FISH (Fig. 6H-K) we found that the majority of secondary TGCs (82.3%) express L1 RNA from the Xi and Xa (Fig. 6K) with a pattern very similar to that observed in ES cells around day 4 of differentiation (Chow et al., 2010). We also examined the methylation status of specific L1 promoters. Two X-linked L1-Tf elements (1 and 2) that are located upstream and downstream of *Huwe1*, respectively, were analyzed and revealed much lower levels of methylation in TGCs compared with somatic tissues or E7.0 embryos (supplementary material Fig. S3B), consistent with their expression in TGCs. No differences were seen between male and female TGCs.

Altogether, these results demonstrate that the Xi not only displays an unusual chromatin status but also an unusual nuclear organization in primary and secondary TGCs, with the absence of an overt silent *Xist* RNA compartment and incomplete exclusion of RNA Pol II. Overall, there are no or few epigenetic characteristics of the Xi in TGCs, other than an enrichment of the PRC2 complex and the H3K27me3 mark. The general lack of DNA methylation at promoters and L1 elements, the presence of certain euchromatic histone modifications and of RNA Pol II, as well as the disrupted *Xist* RNA compartment, are all consistent with the high degree of transcription found for X-linked genes in TGCs.

DISCUSSION

XCI is a dynamic process during early female development. The timing and stability of X-linked gene silencing at different stages of embryogenesis have not been thoroughly explored. In

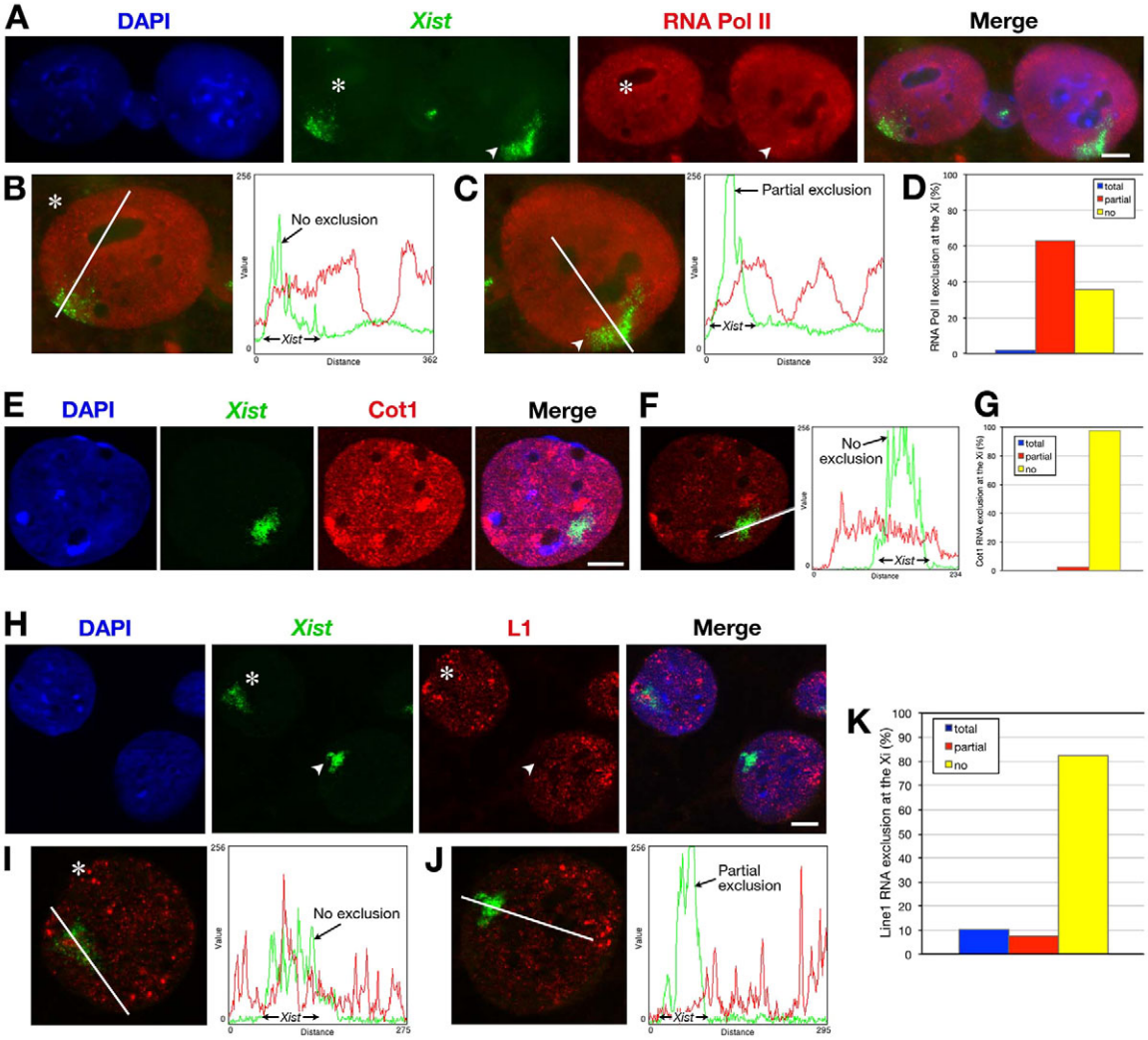

Fig. 6. Absence of a silent *Xist* RNA nuclear compartment in secondary female TGCs derived from E7 EPCs. (**A-D**) RNA Pol II immunofluorescence and *Xist* RNA FISH. (A) Two nuclei showing DAPI staining (blue), RNA Pol II (red) and *Xist* RNA (green). (B) No exclusion of RNA Pol II at the Xi (asterisk). (C) Partial exclusion of RNA Pol II (arrowhead) in the *Xist* RNA domain. (D) Quantification (percentage) of TGCs exhibiting total, partial or no exclusion of RNA Pol II (n=59). (**E-G**) Cot1 and *Xist* RNA FISH. (E) Nucleus stained with DAPI showing no Cot1 (red) hole in the *Xist* RNA domain (green). (F) Presence of Cot1 RNA in the *Xist* RNA domain. (G) Quantification (percentage) of TGCs exhibiting total, partial or no depletion of Cot1 RNA (n=108). (**H-K**) LINE-1 (L1) and *Xist* RNA FISH. (H) Two nuclei showing DAPI staining, *Xist* RNA (green) and L1 RNA (red). (I) No exclusion of L1 at the Xi (asterisk). (J) Partial exclusion of L1 (arrowhead) in the *Xist* RNA domain. (K) Quantification (percentage) of TGCs exhibiting total, partial or no exclusion of L1 (n=68). Solid lines indicate line scan analysis. Scale bars: 10 μm.

previous work, we focused on XCI dynamics in preimplantation embryos (Okamoto et al., 2004; Okamoto et al., 2005; Patrat et al., 2009). In the present study, we investigated the transcriptional status of several endogenous X-linked genes in early E6.5-8.0 postimplantation female mouse embryos using single-cell approaches. We find that genes on the Xi are generally stably silent in embryonic lineages. However, increasing levels of biallelic expression were found for several genes (*Rnf12*, *Mecp2*, *Kif4*, *Atrx*, *Huwe1*) mainly in TGCs. Escape from XCI in TGCs is consistent with a previous study of an X-linked *GFP* transgene (Hadjantonakis et al., 2001). We also show that although most of the genes examined exhibit some degree of XCI escape in secondary TGCs, others (*G6pd*) do not. The patterns of *in vivo* X-linked gene activity we describe here should provide a useful resource as a faithful readout of Xi status. Our results also raise important questions concerning dosage compensation in TGCs and the basis for the epigenetic instability of Xi in these cells.

The TGC lineage is diverse, but two main cell types have been defined, as primary and secondary TGCs (Hemberger, 2008; El-Hashash et al., 2010), arising at different stages of embryogenesis. The murine blastocyst cavity is surrounded by the trophectoderm, which develops into these different types of trophoblast cells after implantation. The polar trophectoderm overlies the ICM and ultimately gives rise to secondary TGCs. It also produces TS cells when cultured under appropriate conditions (Rugg-Gunn et al., 2010). The mural trophectoderm surrounding the rest of the blastocyst differentiates into primary TGCs shortly after implantation. During development, primary TGCs form an anastomosing network of blood sinuses at the periphery of the embryo and facilitate the diffusion of oxygen and nutrients from the maternal circulation into the embryo

(Bevilacqua and Abrahamsohn, 1988). Both the primary and secondary TGCs are believed to play crucial roles in development – for implantation and for the formation of the placenta. Primary TGCs can also develop from blastocyst grown *in vitro* (Carney et al., 1993). Secondary TGCs arise from the polar trophectoderm-derived EPC from ~E7-7.5 onward, and later form the outermost layer of the chorioallantoic placenta (Copp, 1979; Cross, 2000). The central cells of the EPC differentiate into the spongiotrophoblast that forms the intermediate layer of the placenta and secondary TGCs (Cross, 2000). Spontaneous differentiation of cultured EPCs to secondary TGCs has been reported (El-Hashash and Kimber, 2004).

Our finding in both primary and secondary TGCs that X-linked genes can escape silencing is intriguing, as trophoblast development is thought to be extremely sensitive to disruption of normal XCI patterns and is impaired in situations of increased or reduced X-linked gene dosage (reviewed by Hemberger, 2002). Indeed, the X chromosome harbors several housekeeping genes and a high proportion of genes involved in extra-embryonic growth. For example, embryos with two maternal X chromosomes that cannot undergo XCI due to the early maternal imprint preventing *Xist* expression die soon after implantation, primarily owing to severe defects in their extra-embryonic tissues, suggesting that the presence of multiple copies of the Xa is extremely deleterious to development of the extra-embryonic lineages (Shao and Takagi, 1990; Tada et al., 1993; Goto and Takagi, 1998). The importance of dosage compensation in TGCs is also supported by the early postimplantation lethality observed in female embryos carrying mutant *Xist* alleles that fail to undergo imprinted XCI (Marahrens et al., 1997; Hoki et al., 2011), as well as in PRC2 (*Eed*) mutants (Wang et al., 2001) in which defects in extra-embryonic tissues and the absence of correct TGC development have been reported. Indeed, female $Eed^{-/-}$ embryos reactivate their Xp only in differentiating trophoblast cells in the EPC (Kalantry et al., 2006) and this is believed to cause early lethality.

A recent study (Mugford et al., 2012) reported that the poor trophectoderm development in E6.5 embryos with a paternal *Xist* deletion is due to premature differentiation and depletion of Cdx2-positive trophoblast progenitors, rather than to TGC growth and differentiation defects. However, another study (Hoki et al., 2011) showed that the development of secondary TGCs is impaired in the context of an *Xist* hypomorph that survives to E12.5. Thus, disruption of XCI may perturb development to different extents depending on the time window. Our study demonstrates that X-chromosome dosage compensation requirements in TGCs may also vary depending on the gene in question. Although most genes examined showed some degree of XCI escape in TGCs, *G6pd* showed very stable silencing. As *G6pd* is a housekeeping gene, perturbations in its expression levels could have a serious impact on extra-embryonic development (reviewed by Hemberger, 2007) and mechanisms to ensure the more stable silencing of such genes, in the otherwise 'relaxed' epigenetic environment in TGCs, might have evolved.

Xist RNA plays a key role in XCI in both extra-embryonic and embryonic lineages. A recent study using an inducible *Tsix* transgene to repress *Xist* at different stages of development revealed that there is a requirement for *Xist* RNA to maintain X-linked GFP silencing much later in extra-embryonic development than previously suspected (Ohhata et al., 2011). One of the proposed roles of *Xist* RNA in XCI is the formation of a silent nuclear compartment depleted of RNA Pol II and Cot1 RNA (Chaumeil et al., 2006). Our findings reveal that, despite the presence of *Xist* RNA, the silent compartment is severely disrupted in TGCs, with the presence of RNA Pol II and euchromatin marks such as histone acetylation and H3K4 methylation. Together with the lack of promoter DNA methylation, this reorganization of the Xi might participate in the epigenetic instability observed on the Xi in TGCs. This relaxed epigenetic state of the Xi could be partly due to the fact that TGCs undergo endoreplication (Simmons et al., 2007), i.e. the S and G phases of the cell cycle without mitosis, resulting in increased gene expression through polyploidy (reviewed by Lee et al., 2009). Repeated replication cycles without mitosis might result in the gradual disorganization of the silent nuclear compartment that had initially been created by *Xist* RNA in the trophectoderm of the blastocyst. This might in turn result in the unusual combination of active and inactive chromatin marks that is associated with the Xi in TGCs. Nevertheless, PRC2 and H3K27me3 remain on the Xi, despite the presence of RNA Pol II and euchromatic marks, suggesting that the loss of transcriptional activity is not a prerequisite for PRC2 association, at least in TGCs.

Xi lability in TGCs could also be due to the low levels of DNA methylation at the CpG islands of genes. DNA methylation plays an important role in stabilizing the inactive state in somatic cells (Lock et al., 1987; Singer-Sam et al., 1990; Grant et al., 1992) and global methylated DNA immunoprecipitation studies have revealed that CpG islands of X-linked genes are hypermethylated on the Xi in somatic cells (Weber et al., 2005). However, extra-embryonic tissues are thought to exhibit reduced methylation, particularly at promoters of X-linked genes (Kratzer et al., 1983; Sado et al., 2000). Moreover, a recent report clearly shows that extra-embryonic, and specifically trophoblast, cell types can form in the absence of DNA methylation (Sakaue et al., 2010). All of the X-linked genes that we analyzed, including *G6pd*, displayed reduced DNA methylation levels in TGCs compared with somatic tissues. Thus, although DNA hypomethylation might contribute to the epigenetic instability in TGCs, it cannot be responsible for the differences in the degree of silencing that we observed between genes. The extent to which the genes that we analyzed are dependent on *Xist* RNA or PRC2 for their silencing, albeit partial, and whether other marks are responsible for the inactivity of *G6pd*, will be important questions for the future.

In conclusion, we demonstrate that in primary and secondary TGCs the Xi has an unusual chromosome organization, with both active and inactive features. This apparent 'bivalence' in Xi chromatin might account for the significant degree of epigenetic instability and escape from XCI that we observe. However, the fact that not all genes show a relaxed expression status indicates that key loci might require dosage compensation in TGCs and points to as yet undefined mechanisms for maintaining silencing at such loci in an otherwise labile environment.

Acknowledgements

We thank Dr Julie Chaumeil for critical reading of the manuscript; Sophie Gournet for help with illustrations; and members of the E.H. laboratory for critical discussions and feedback. The help of the Animal Housing Facility and the Imaging Platform of the Unit are also gratefully acknowledged.

Funding

This work was supported by the Fondation pour la Recherche Médicale (Equipe FRM); the Agence Nationale de la Recherche (ANR); the EpiGeneSys FP7 no. 257082 Network of Excellence to E.H.; a European Research Council (ERC) Advanced Investigator Award [no. 250367] and EU FP7 SYBOSS [grant no. 242129] to E.H.

Competing interests statement
The authors declare no competing financial interests.

Supplementary material
Supplementary material available online at
http://dev.biologists.org/lookup/suppl/doi:10.1242/dev.087429/-/DC1

References

Augui, S., Nora, E. P. and Heard, E. (2011). Regulation of X-chromosome inactivation by the X-inactivation centre. *Nat. Rev. Genet.* **12**, 429-442.
Baumann, C. and De La Fuente, R. (2009). ATRX marks the inactive X chromosome (Xi) in somatic cells and during imprinted X chromosome inactivation in trophoblast stem cells. *Chromosoma* **118**, 209-222.
Bevilacqua, E. M. and Abrahamsohn, P. A. (1988). Ultrastructure of trophoblast giant cell transformation during the invasive stage of implantation of the mouse embryo. *J. Morphol.* **198**, 341-351.
Carney, E. W., Prideaux, V., Lye, S. J. and Rossant, J. (1993). Progressive expression of trophoblast-specific genes during formation of mouse trophoblast giant cells in vitro. *Mol. Reprod. Dev.* **34**, 357-368.
Chaumeil, J., Okamoto, I., Guggiari, M. and Heard, E. (2002). Integrated kinetics of X chromosome inactivation in differentiating embryonic stem cells. *Cytogenet. Genome Res.* **99**, 75-84.
Chaumeil, J., Le Baccon, P., Wutz, A. and Heard, E. (2006). A novel role for Xist RNA in the formation of a repressive nuclear compartment into which genes are recruited when silenced. *Genes Dev.* **20**, 2223-2237.
Chaumeil, J., Augui, S., Chow, J. C. and Heard, E. (2008). Combined immunofluorescence, RNA fluorescent in situ hybridization, and DNA fluorescent in situ hybridization to study chromatin changes, transcriptional activity, nuclear organization, and X-chromosome inactivation. *Methods Mol. Biol.* **463**, 297-308.
Chow, J. C., Ciaudo, C., Fazzari, M. J., Mise, N., Servant, N., Glass, J. L., Attreed, M., Avner, P., Wutz, A., Barillot, E. et al. (2010). LINE-1 activity in facultative heterochromatin formation during X chromosome inactivation. *Cell* **141**, 956-969.
Copp, A. J. (1979). Interaction between inner cell mass and trophectoderm of the mouse blastocyst. II. The fate of the polar trophectoderm. *J. Embryol. Exp. Morphol.* **51**, 109-120.
Corbel, C., Salaün, J., Belo-Diabangouaya, P. and Dieterlen-Lièvre, F. (2007). Hematopoietic potential of the pre-fusion allantois. *Dev. Biol.* **301**, 478-488.
Cross, J. C. (2000). Genetic insights into trophoblast differentiation and placental morphogenesis. *Semin. Cell Dev. Biol.* **11**, 105-113.
Csankovszki, G., Nagy, A. and Jaenisch, R. (2001). Synergism of Xist RNA, DNA methylation, and histone hypoacetylation in maintaining X chromosome inactivation. *J. Cell Biol.* **153**, 773-784.
Downs, K. M. and Davies, T. (1993). Staging of gastrulating mouse embryos by morphological landmarks in the dissecting microscope. *Development* **118**, 1255-1266.
Ehrich, M., Nelson, M. R., Stanssens, P., Zabeau, M., Liloglou, T., Xinarianos, G., Cantor, C. R., Field, J. K. and van den Boom, D. (2005). Quantitative high-throughput analysis of DNA methylation patterns by base-specific cleavage and mass spectrometry. *Proc. Natl. Acad. Sci. USA* **102**, 15785-15790.
El-Hashash, A. H. and Kimber, S. J. (2004). Trophoblast differentiation in vitro: establishment and characterisation of a serum-free culture model for murine secondary trophoblast giant cells. *Reproduction* **128**, 53-71.
El-Hashash, A. H., Warburton, D. and Kimber, S. J. (2010). Genes and signals regulating murine trophoblast cell development. *Mech. Dev.* **127**, 1-20.
Escamilla-Del-Arenal, M., da Rocha, S. T. and Heard, E. (2011). Evolutionary diversity and developmental regulation of X-chromosome inactivation. *Hum. Genet.* **130**, 307-327.
Garrick, D., Sharpe, J. A., Arkell, R., Dobbie, L., Smith, A. J. H., Wood, W. G., Higgs, D. R. and Gibbons, R. J. (2006). Loss of Atrx affects trophoblast development and the pattern of X-inactivation in extraembryonic tissues. *PLoS Genet.* **2**, e58.
Goto, Y. and Takagi, N. (1998). Tetraploid embryos rescue embryonic lethality caused by an additional maternally inherited X chromosome in the mouse. *Development* **125**, 3353-3363.
Grant, M., Zuccotti, M. and Monk, M. (1992). Methylation of CpG sites of two X-linked genes coincides with X-inactivation in the female mouse embryo but not in the germ line. *Nat. Genet.* **2**, 161-166.
Hadjantonakis, A.-K., Cox, L. L., Tam, P. P. L. and Nagy, A. (2001). An X-linked GFP transgene reveals unexpected paternal X-chromosome activity in trophoblastic giant cells of the mouse placenta. *Genesis* **29**, 133-140.
Hall, L. L. and Lawrence, J. B. (2011). XIST RNA and architecture of the inactive X chromosome: implications for the repeat genome. *Cold Spring Harb. Symp. Quant. Biol.* **75**, 345-356.
Hemberger, M. (2002). The role of the X chromosome in mammalian extra embryonic development. *Cytogenet. Genome Res.* **99**, 210-217.
Hemberger, M. (2007). Epigenetic landscape required for placental development. *Cell. Mol. Life Sci.* **64**, 2422-2436.
Hemberger, M. (2008). IFPA award in placentology lecture - characteristics and significance of trophoblast giant cells. *Placenta* **29 Suppl. A**, 4-9.
Hoki, Y., Ikeda, R., Mise, N., Sakata, Y., Ohhata, T., Sasaki, H., Abe, K. and Sado, T. (2011). Incomplete X-inactivation initiated by a hypomorphic Xist allele in the mouse. *Development* **138**, 2649-2659.
Hu, D. and Cross, J. C. (2010). Development and function of trophoblast giant cells in the rodent placenta. *Int. J. Dev. Biol.* **54**, 341-354.
Jeppesen, P. and Turner, B. M. (1993). The inactive X chromosome in female mammals is distinguished by a lack of histone H4 acetylation, a cytogenetic marker for gene expression. *Cell* **74**, 281-289.
Kalantry, S., Mills, K. C., Yee, D., Otte, A. P., Panning, B. and Magnuson, T. (2006). The Polycomb group protein Eed protects the inactive X-chromosome from differentiation-induced reactivation. *Nat. Cell Biol.* **8**, 195-202.
Keohane, A. M., O'neill, L. P., Belyaev, N. D., Lavender, J. S. and Turner, B. M. (1996). X-Inactivation and histone H4 acetylation in embryonic stem cells. *Dev. Biol.* **180**, 618-630.
Kratzer, P. G., Chapman, V. M., Lambert, H., Evans, R. E. and Liskay, R. M. (1983). Differences in the DNA of the inactive X chromosomes of fetal and extraembryonic tissues of mice. *Cell* **33**, 37-42.
Lee, H. O., Davidson, J. M. and Duronio, R. J. (2009). Endoreplication: polyploidy with purpose. *Genes Dev.* **23**, 2461-2477.
Lock, L. F., Takagi, N. and Martin, G. R. (1987). Methylation of the Hprt gene on the inactive X occurs after chromosome inactivation. *Cell* **48**, 39-46.
Ma, G. T. and Linzer, D. I. H. (2000). GATA-2 restricts prolactin-like protein A expression to secondary trophoblast giant cells in the mouse. *Biol. Reprod.* **63**, 570-574.
Mak, W., Nesterova, T. B., de Napoles, M., Appanah, R., Yamanaka, S., Otte, A. P. and Brockdorff, N. (2004). Reactivation of the paternal X chromosome in early mouse embryos. *Science* **303**, 666-669.
Marahrens, Y., Panning, B., Dausman, J., Strauss, W. and Jaenisch, R. (1997). Xist-deficient mice are defective in dosage compensation but not spermatogenesis. *Genes Dev.* **11**, 156-166.
Mugford, J. W., Yee, D. and Magnuson, T. (2012). Failure of extra-embryonic progenitor maintenance in the absence of dosage compensation. *Development* **139**, 2130-2138.
Ohhata, T., Senner, C. E., Hemberger, M. and Wutz, A. (2011). Lineage-specific function of the noncoding *Tsix* RNA for Xist repression and Xi reactivation in mice. *Genes Dev.* **25**, 1702-1715.
Okamoto, I., Otte, A. P., Allis, C. D., Reinberg, D. and Heard, E. (2004). Epigenetic dynamics of imprinted X inactivation during early mouse development. *Science* **303**, 644-649.
Okamoto, I., Arnaud, D., Le Baccon, P., Otte, A. P., Disteche, C. M., Avner, P. and Heard, E. (2005). Evidence for de novo imprinted X-chromosome inactivation independent of meiotic inactivation in mice. *Nature* **438**, 369-373.
Patrat, C., Okamoto, I., Diabangouaya, P., Vialon, V., Le Baccon, P., Chow, J. and Heard, E. (2009). Dynamic changes in paternal X-chromosome activity during imprinted X-chromosome inactivation in mice. *Proc. Natl. Acad. Sci. USA* **106**, 5198-5203.
Penny, G. D., Kay, G. F., Sheardown, S. A., Rastan, S. and Brockdorff, N. (1996). Requirement for Xist in X chromosome inactivation. *Nature* **379**, 131-37.
Rastan, S. (1982). Timing of X-chromosome inactivation in postimplantation mouse embryos. *J. Embryol. Exp. Morphol.* **71**, 11-24.
Rugg-Gunn, P. J., Cox, B. J., Ralston, A. and Rossant, J. (2010). Distinct histone modifications in stem cell lines and tissue lineages from the early mouse embryo. *Proc. Natl. Acad. Sci. USA* **107**, 10783-10790.
Sado, T., Fenner, M. H., Tan, S.-S., Tam, P., Shioda, T. and Li, E. (2000). X inactivation in the mouse embryo deficient for Dnmt1: distinct effect of hypomethylation on imprinted and random X inactivation. *Dev. Biol.* **225**, 294-303.
Sakaue, M., Ohta, H., Kumaki, Y., Oda, M., Sakaide, Y., Matsuoka, C., Yamagiwa, A., Niwa, H., Wakayama, T. and Okano, M. (2010). DNA methylation is dispensable for the growth and survival of the extraembryonic lineages. *Curr. Biol.* **20**, 1452-1457.
Shao, C. and Takagi, N. (1990). An extra maternally derived X chromosome is deleterious to early mouse development. *Development* **110**, 969-975.
Simmons, D. G., Fortier, A. L. and Cross, J. C. (2007). Diverse subtypes and developmental origins of trophoblast giant cells in the mouse placenta. *Dev. Biol.* **304**, 567-578.
Singer-Sam, J., Grant, M., LeBon, J. M., Okuyama, K., Chapman, V., Monk, M. and Riggs, A. D. (1990). Use of a HpaII-polymerase chain reaction assay to study DNA methylation in the Pgk-1 CpG island of mouse embryos at the time of X-chromosome inactivation. *Mol. Cell. Biol.* **10**, 4987-4989.
Tada, T., Takagi, N. and Adler, I. D. (1993). Parental imprinting on the mouse X chromosome: effects on the early development of X0, XXY and XXX embryos. *Genet. Res.* **62**, 139-148.

Takagi, N., Sugawara, O. and Sasaki, M. (1982). Regional and temporal changes in the pattern of X-chromosome replication during the early post-implantation development of the female mouse. *Chromosoma* **85**, 275-286.
Tan, S. S., Williams, E. A. and Tam, P. P. (1993). X-chromosome inactivation occurs at different times in different tissues of the post-implantation mouse embryo. *Nat. Genet.* **3**, 170-174.
Wang, J., Mager, J., Chen, Y., Schneider, E., Cross, J. C., Nagy, A. and Magnuson, T. (2001). Imprinted X inactivation maintained by a mouse Polycomb group gene. *Nat. Genet.* **28**, 371-375.
Weber, M., Davies, J. J., Wittig, D., Oakeley, E. J., Haase, M., Lam, W. L. and Schübeler, D. (2005). Chromosome-wide and promoter-specific analyses identify sites of differential DNA methylation in normal and transformed human cells. *Nat. Genet.* **37**, 853-862.
Williams, L. H., Kalantry, S., Starmer, J. and Magnuson, T. (2011). Transcription precedes loss of Xist coating and depletion of H3K27me3 during X-chromosome reprogramming in the mouse inner cell mass. *Development* **138**, 2049-2057.
Wutz, A. (2011). Gene silencing in X-chromosome inactivation: advances in understanding facultative heterochromatin formation. *Nat. Rev. Genet.* **12**, 542-553.
Zybina, E. V. and Zybina, T. G. (1996). Polytene chromosomes in mammalian cells. *Int. Rev. Cytol.* **165**, 53-119.

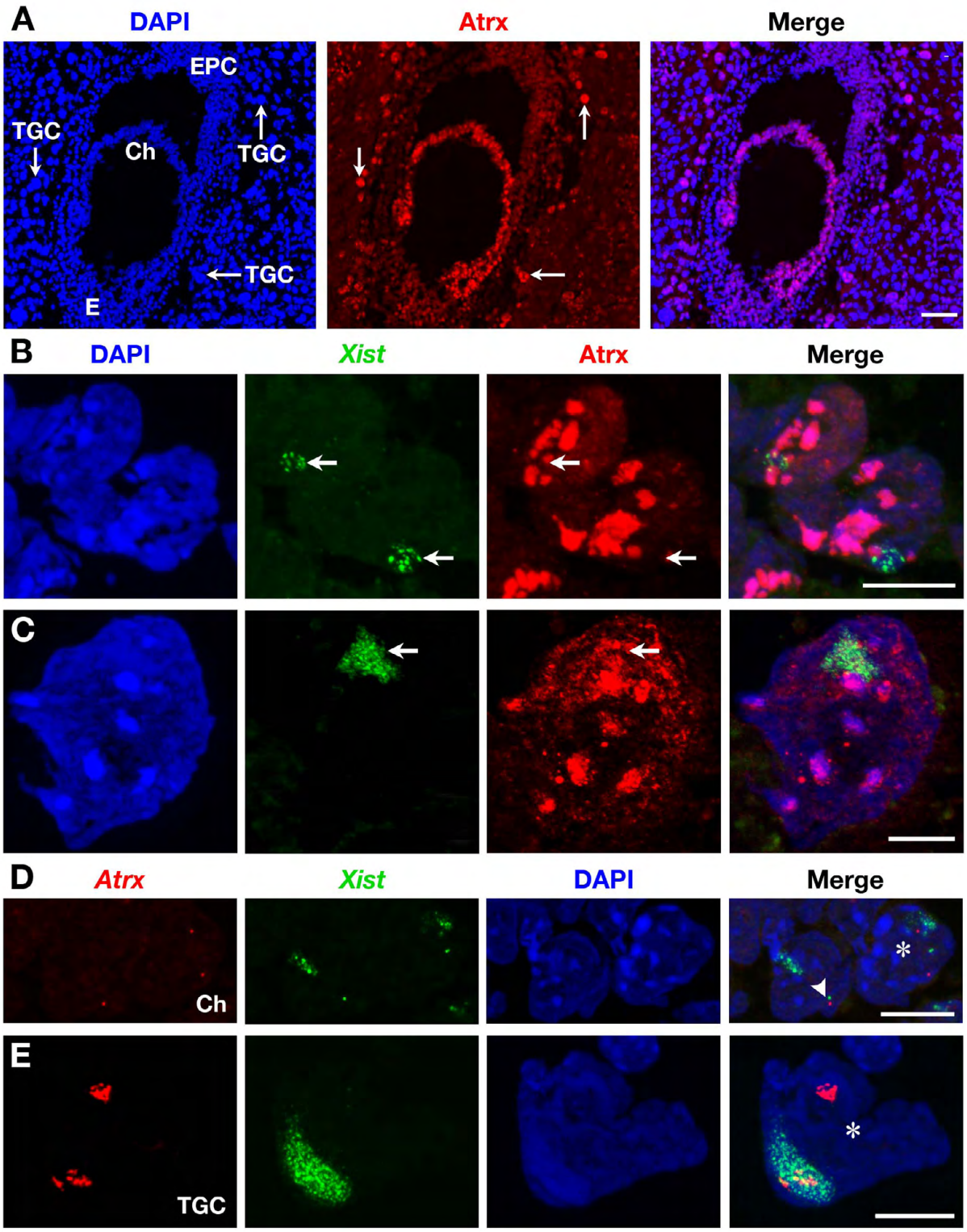

Fig. S1. Atrx protein and *Atrx* RNA expression during imprinted X inactivation of extra-embryonic lineages at the postimplantation stage. (**A**) Longitudinal section of E7 female embryo immunostained with an antibody against Atrx. Scale bar: 100 µm. (**B**,**C**) RNA FISH for *Xist* (green) and immunofluorescence for Atrx (red). (B) Two nuclei from the chorion showing no overlap of the *Xist* domain with the Atrx protein. Only 5.8% (5/86) of nuclei from this extra-embryonic tissue exhibit partial overlap between *Xist* and Atrx. Scale bar: 10 µm. (C) One representative TGC showing *Xist* that partially overlaps with Atrx. They represent 25% (6/24) of TGCs. Scale bar: 100 µm. (**D**,**E**) RNA FISH to detect *Xist* RNA (green) and *Atrx* primary transcripts (red). (D) Two nuclei from E7 female embryonic chorion showing monoallelic (arrowhead) and biallelic (asterisk) *Atrx* expression. Scale bar: 10 µm. (E) One representative TGC showing biallelic *Atrx* expression (asterisk). Scale bar: 100 µm. Ch, chorion; E, embryo; EPC, ectoplacental cone; TGC, trophoblast giant cell.

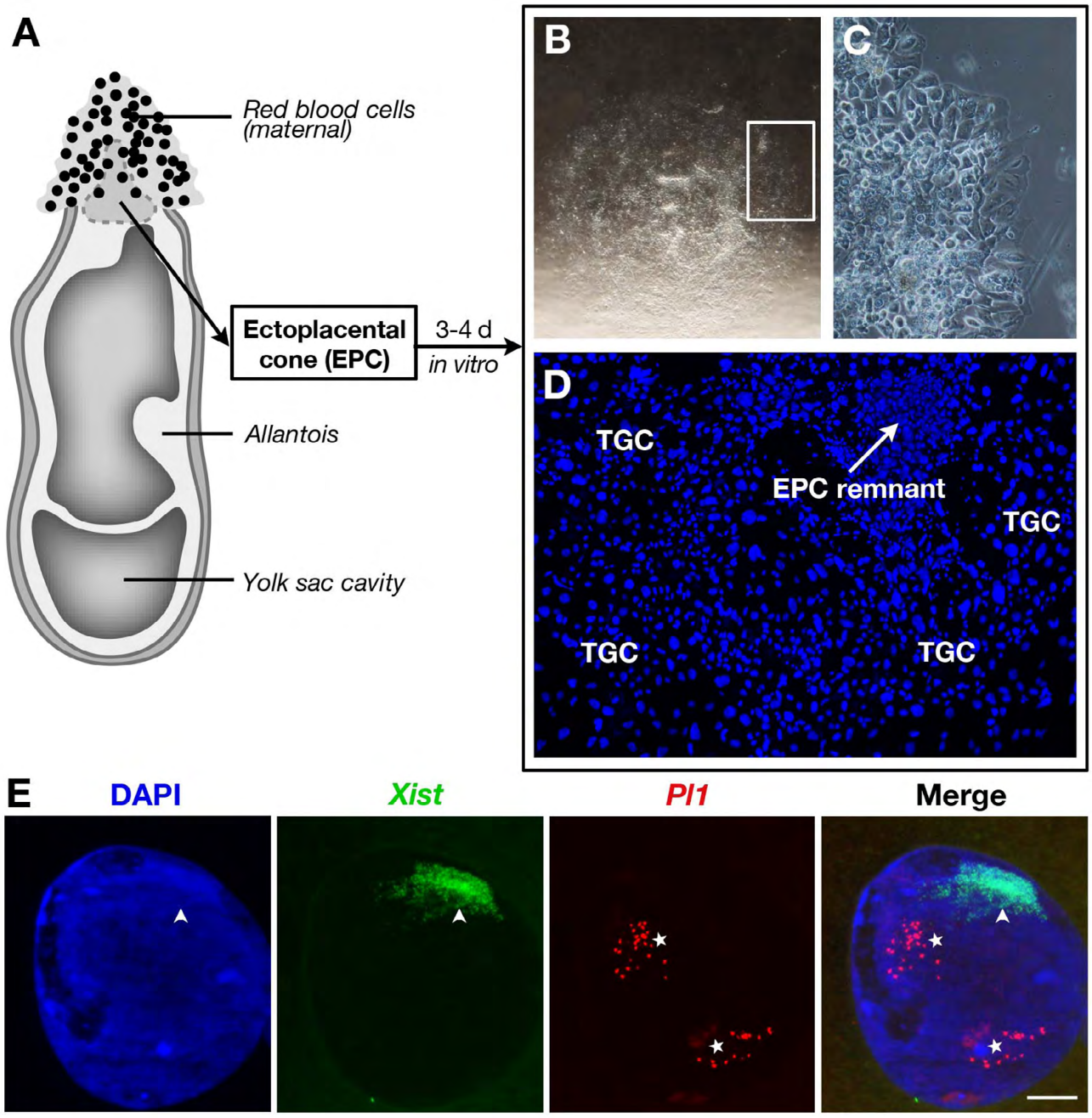

Fig. S2. Secondary TGC differentiation from E7 ectoplacental cone. (**A**) Drawing of an E7 embryo prior to EPC dissection. The EPC was separated from the embryo and yolk sac. It was also deprived of surrounding red blood cells prior to being deposited on a glass coverslip in culture medium. (**B-D**) TGCs developed from an E7 EPC after 3-4 days of culture. Individual explant forms an outgrowth (B) that spreads as a monolayer of flattened TGCs (C). TGC with giant nuclei can be detected, spread around the EPC remnant (arrow), as shown by DAPI staining (D). (**E**) Transcriptional activity of *Pl1* assayed by RNA FISH in secondary female TGC derived from E7 EPC. *Pl1* RNA (red, indicated by a star), a specific marker for TGCs, is detected on chromosome 13, whereas *Xist* RNA (green) accumulates on the X chromosome. Dense DAPI intensity and the *Xist* domain colocalize as indicated by the arrowhead. Scale bar: 10 µm.

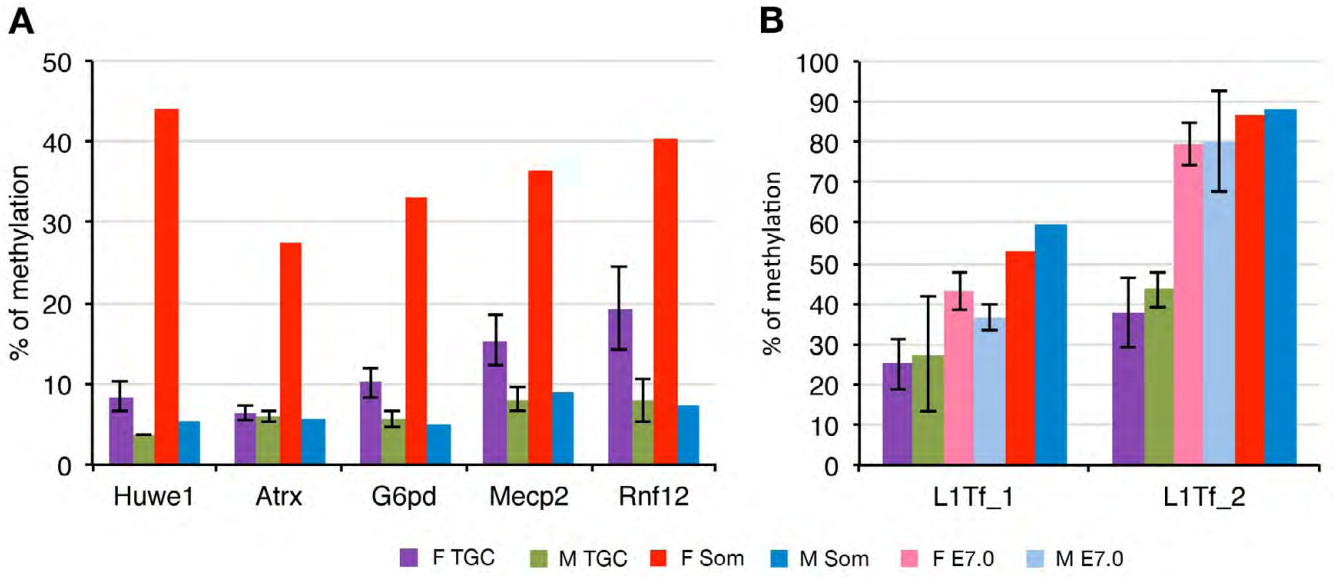

Fig. S3. DNA methylation analysis by bisulfite sequencing of X-linked genes and LINE-1 (Tf) promoters in secondary TGCs. Percentage of methylation in female (F) and male (M) is shown. (**A**) X-linked promoter (*Huwe1*, *Atrx*, *G6pd*, *Mecp2* and *Rnf12*) methylation in secondary TGCs generated from single E7 EPCs cultured for 3 days and somatic tissues (som, adult liver cells). (**B**) Methylation of L1-Tf elements located immediately upstream (1) and downstream (2) of the *Huwe1* gene as described (Chow et al., 2010) in secondary TGCs and somatic tissues.

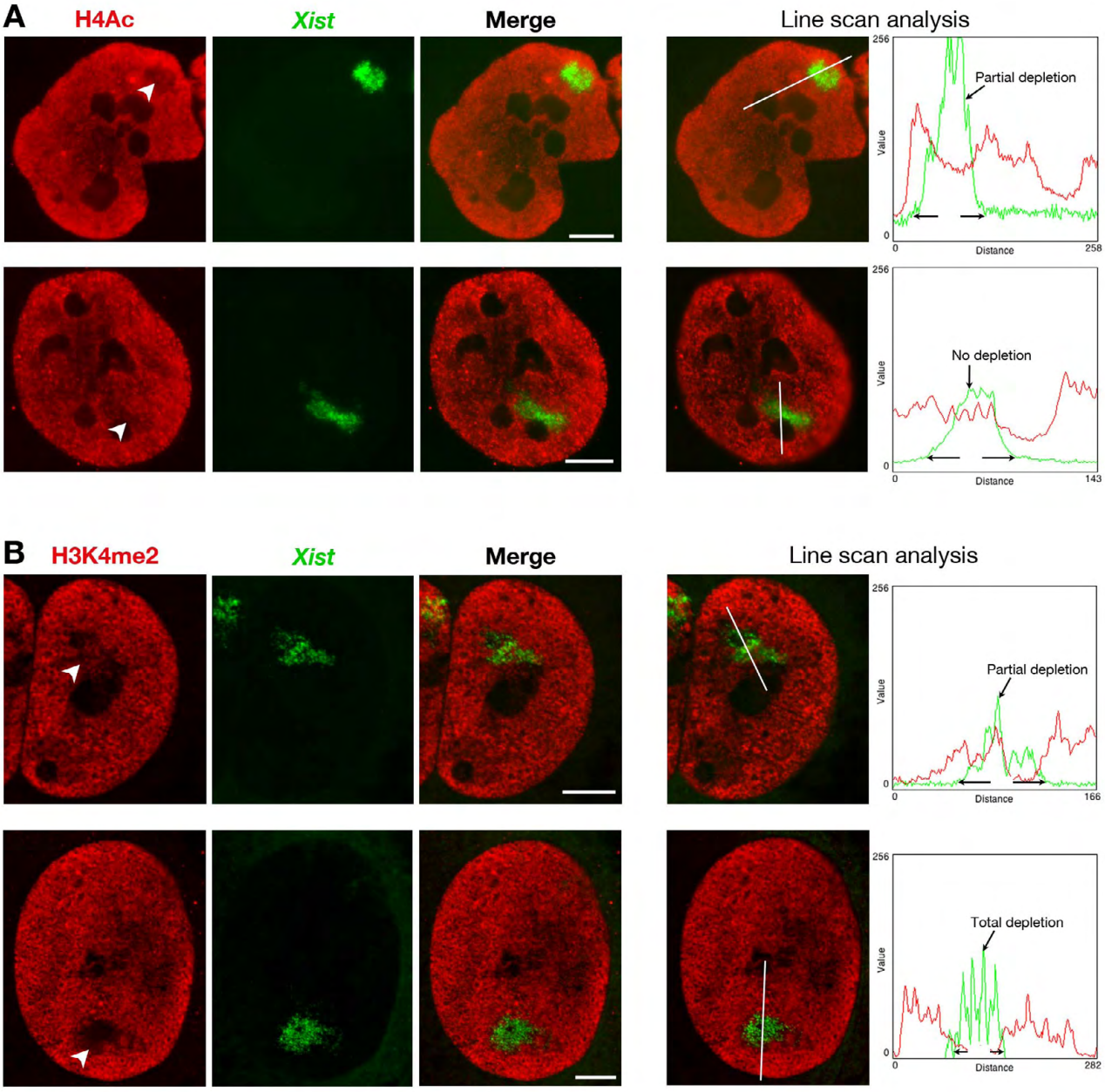

Fig. S4. 3D images and line scan analysis of H4 acetylation and H3K4 dimethylation of secondary TGCs. (**A**) H4 acetylation at the Xi. Upper panel, partial depletion; lower panel, no depletion. (**B**) H3K4 dimethylation at the Xi. Upper panel, partial depletion; lower panel, total depletion.

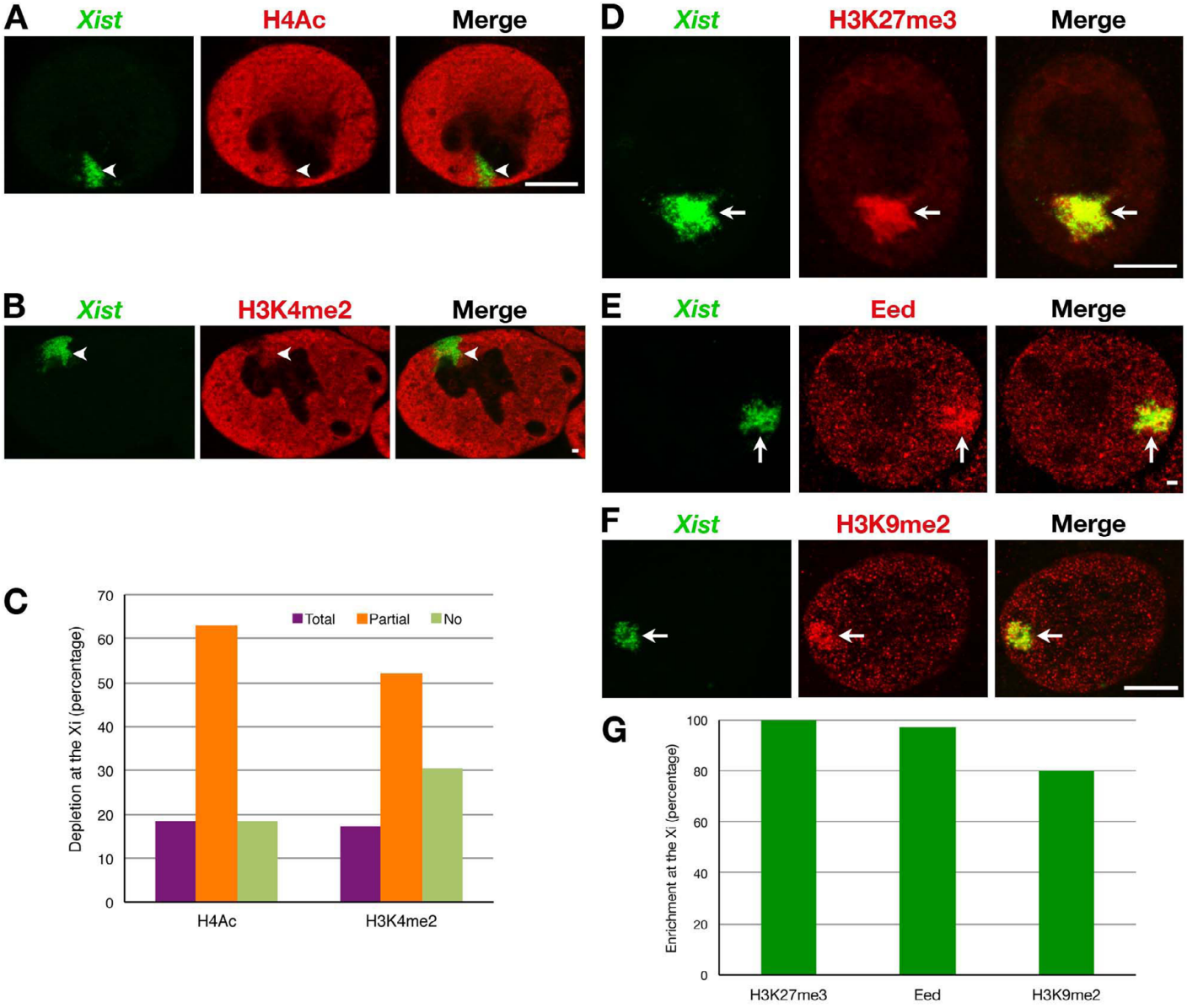

Fig. S5. 3D analysis of active marks (H4 acetylation, H3K4 dimethylation) and repressive marks (H3K27me3 and Eed) of primary female TGCs derived from E3 blastocyst. See Fig 3. (**A**) H4 acetylation at the Xi, showing partial depletion. (**B**) H3K4 dimethylation at the Xi, showing partial depletion. (**C**) Quantification of active marks: H4 acetylation (*n*=38 from four embryos) and H3K4me2 (*n*=46 from five embryos). (**D**) H3K27me3 at the Xi, showing colocalization. (**E**) Eed at the Xi, showing colocalization. (**F**) H3K9me2 at the Xi, showing colocalization. (**G**) Quantification of repressive marks: H3K27me3 (*n*=41 from four embryos), Eed (*n*=61 from four embryos) and H3K9me2 (*n*=20 from one embryo).

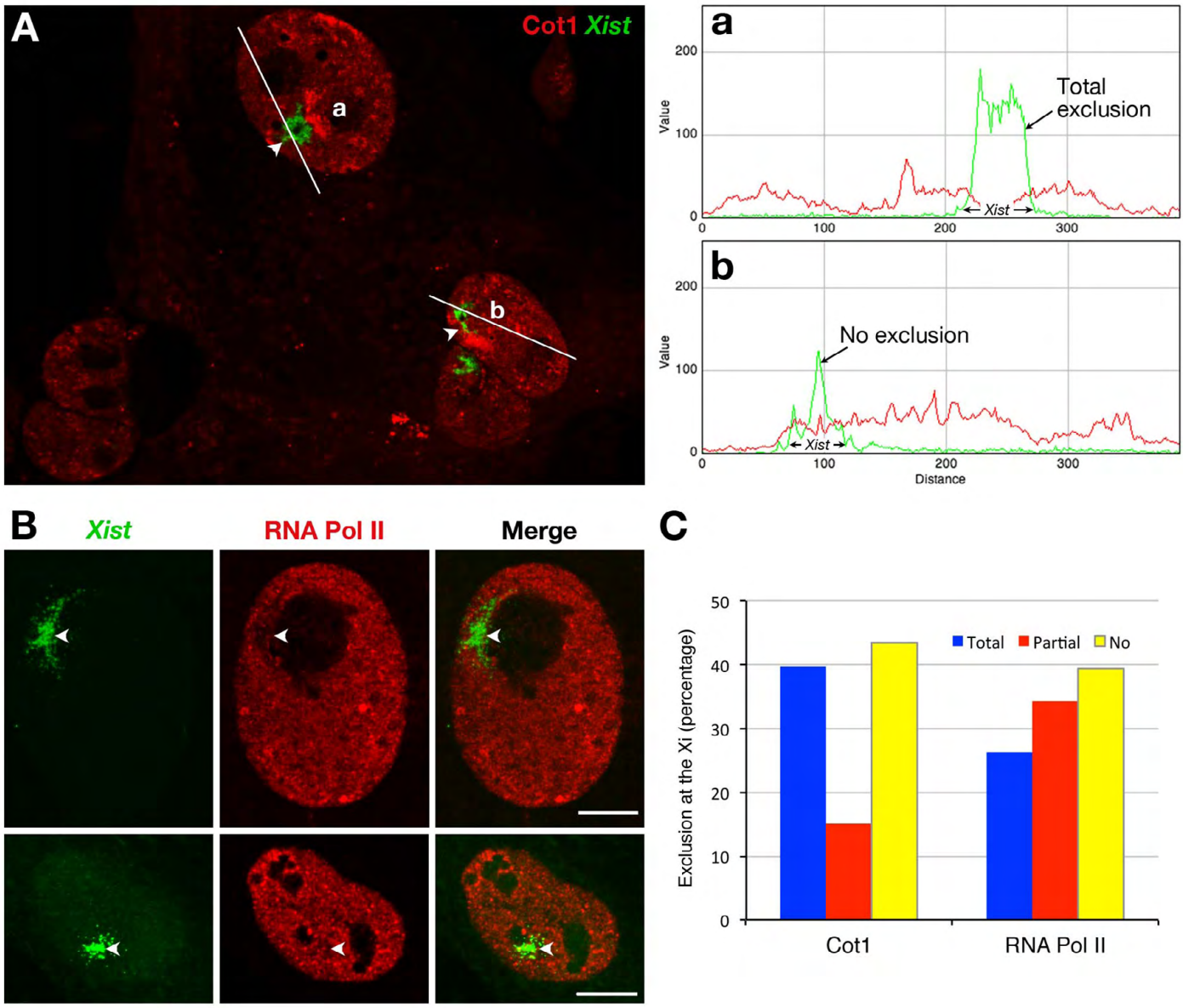

Fig. S6. No silent *Xist* RNA nuclear compartment on the paternal X chromosome in primary TGCs. (**A**) *Cot1* and *Xist* RNA FISH. (**a**,**b**) Representative examples of 3D analysis and line scans showing the total (a) and no (b) exclusion of *Cot1* RNA in the *Xist* RNA domain. (**B**) RNA Pol II immunofluorescence and *Xist* RNA FISH. Exclusion of RNA Pol II (red) in the *Xist* RNA domain (green); upper panel, partial exclusion; lower panel, no exclusion. (**C**) Quantification of primary TGCs exhibiting total, partial or no exclusion of *Cot1* RNA and RNA Pol II. For *Cot1* RNA FISH, three blastocysts were cultured and 12, 12 and 29 primary TGCs were analyzed, respectively (n=53). For RNA Pol II immunofluorescence, five blastocysts were cultured and 1, 5, 14, 20 and 21 primary TGCs were analyzed, respectively (n=61). The results indicate the mean (percentage). Scale bars: 10 μm.

Table S1. Efficiency of RNA primary transcripts for different genes in different cell types in male embryos

Gene	Tissue/cell	Total no. of cells	Expression (%)
Kif4	E7 embryo	90	90
	E7.5 embryo	50	100
	E7 VE	49	79.6
	E7.5 VE	27	96.3
	E7 EPC+Ch	65	87.7
	E7.5 EPC+Ch	9	77.8
	E7 TGC	4	100
Huwe1	E7 embryo	89	97.7
	E7.5 embryo	59	89.8
	E7 VE	74	77.0
	E7.5 VE	65	86.1
	E7 EPC+Ch	73	95.9
	E7.5 EPC+Ch	39	82.1
	E7 TGC	12	100
	E7.5 TGC	8	87.5
	Secondary TGC*	38	100
Atrx	Secondary TGC*	64	95.3
Rnf12	Secondary TGC*	71	98.6
G6pd	Secondary TGC*	37	89.2

VE, visceral endoderm; EPC, ectoplacental cone; Ch, chorion; TGC, trophoblast giant cell.
*Secondary TGC obtained upon 3-4 days of E7 EPC culture.

Table S2. Biallelic expression of X-linked genes in TGCs analyzed on embryo sections at different postimplantation stages

	X-linked genes				
	% of *in vivo* TGCs showing escape (*n*=number of analyzed TGCs/embryo)				
Embryonic stage	*Kif4*	*Rnf12*	*Mecp2*	*Huwe1*	*Atrx*
E6.5	3.1 (*n*=32)	14.3 (*n*=7) 0 (*n*=11)	0 (*n*=2) 17.2 (*n*=29)	14.8 (*n*=27) 0 (*n*=4)	42.8 (*n*=7) 33.3 (*n*=3)
E7.0	0 (*n*=2) 0 (*n*=17) 0 (*n*=16)	10.0 (*n*=10) 5.5 (*n*=18) 25.0 (*n*=4)	25.0 (*n*=8) 25.0 (*n*=12) 0 (*n*=18)	42.3 (*n*=52) 14.3 (*n*=7) 20.0 (*n*=10)	33.3 (*n*=15) 22.2 (*n*=9) 37.5 (*n*=8) 33.3 (*n*=15)
E7.5	21.4 (*n*=14) 16.7 (*n*=12)	0 (*n*=14) 20 (*n*=25) 16.6 (*n*=18)	27.8 (*n*=18) 23.5 (*n*=17)	15.4 (*n*=13) 28.6 (*n*=28)	24.0 (*n*=25) 42.3 (*n*=26)
E8.0	14.3 (*n*=21) 35.7 (*n*=14)	25.9 (*n*=27) 40.0 (*n*=10)	11.1 (*n*=18) 45.4 (*n*=11)	27.3 (*n*=11) 20.0 (*n*=10)	52.6 (*n*=19) 28.6 (*n*=7) 55.2 (*n*=29)

Table S3. Primer information for Sequenom epityper analysis [sequence, annealing temperature (Ta) and product size]

ID	Primer	Sequence	Ta (°C)	Size (bp)
Huwe1	Huwe1_F	GAGATTTTATGTTTTTTAAAGG	60	329
	Huwe1_R	ACTCCTACACTCAATAACCAACCTC		
Atrx	Atrx_F	TTAAGTTTTAGTTGGGGTTTTTTAT	60	313
	Atrx_R	ATAACTACTAAAATCCCAATACTTTTC		
G6pdx	G6pdx_F	GGAAAGTTAGGTTATATATAATGGTTGG	58	490
	G6pdx_R	AATCTAATCCTCATAAACCCAATAC		
Mecp2	Mecp2_F	GAGGAGGAGGGAGTAAAATTTAGAG	60	296
	Mecp2_R	CATCCTAAACCCCAACTATACAAAC		
Rnf12	Rnf12_F	TTTTATTTTATTTTTTTAAATTTTAGTT	60	459
	Rnf12_R	AACCCAATTAAATTCCCTCCTAAC		
Tf-1	Tf-1_F	AGGTTTTTGAAGTTTATTGAGAGTT	58	342
	Tf-1_R	TATTCAAACTAATTTCCTAAATCCC		
Tf-2	Tf-2_F	AGTAGAGGTTTTAAAAATTTAATTTTTAGT	55	313
	Tf-2_R	CAAAAAATCCTAAAACCAAAATAAC		
	10bp 5'tag	AGGAAGAGAG		
	T7 3'tag	CAGTAATACGACTCACTATAGGGAGAAGGCT		